AD NUMBER

AD862102

LIMITATION CHANGES

TO:

Approved for public release; distribution is unlimited.

FROM:

Distribution authorized to U.S. Gov't. agencies and their contractors; Critical Technology; AUG 1969. Other requests shall be referred to Army Aviation Materiel Laboratories, Fort Eustis, VA 23604. This document contains export-controlled technical data.

AUTHORITY

USAAMRDL ltr dtd 23 Jun 1971

AD

USAAVLABS TECHNICAL REPORT 69-60

THE MAXIMUM STRENGTH OF INITIALLY IMPERFECT, AXIALLY COMPRESSED, CIRCULAR CYLINDRICAL SHELLS

By

J. Mayers
D. L. Wesenberg

August 1969

U. S. ARMY AVIATION MATERIEL LABORATORIES
FORT EUSTIS, VIRGINIA

CONTRACT DAAJ02-68-C-0037
DEPARTMENT OF AERONAUTICS AND ASTRONAUTICS
STANFORD UNIVERSITY
STANFORD, CALIFORNIA

DEPARTMENT OF THE ARMY
HEADQUARTERS US ARMY AVIATION MATERIEL LABORATORIES
FORT EUSTIS, VIRGINIA 23604

This program was carried out under Contract DAAJ02-68-C-0035 with Stanford University.

The data contained in this report are the result of research conducted to investigate the maximum strength of initially imperfect, axially compressed, circular cylindrical shells with the use of Reissner's variational principle modified to include the effects of nonlinear-elastic material behavior. Families of load-shortening curves are presented for various radius-to-thickness ratios for several materials.

The report has been reviewed by the U. S. Army Aviation Materiel Laboratories and is considered to be technically sound. It is published for the exchange of information and the stimulation of future research.

Disclaimers

The findings in this report are not to be construed as an official Department of the Army position unless so designated by other authorized documents.

When Government drawings, specifications, or other data are used for any purpose other than in connection with a definitely related Government procurement operation, the United States Government thereby incurs no responsibility nor any obligation whatsoever; and the fact that the Government may have formulated, furnished, or in any way supplied the said drawings, specifications, or other data is not to be regarded by implication or otherwise as in any manner licensing the holder or any other person or corporation, or conveying any rights or permission, to manufacture, use, or sell any patented invention that may in any way be related thereto.

Disposition Instructions

Destroy this report when no longer needed. Do not return it to the originator.

Task 1F162204A17002
Contract DAAJ02-68-C-0035
USAAVLABS Technical Report 69-60
August 1969

THE MAXIMUM STRENGTH OF INITIALLY IMPERFECT, AXIALLY COMPRESSED, CIRCULAR CYLINDRICAL SHELLS

Final Report

By
J. Mayers and D. L. Wesenberg

Prepared by

Department of Aeronautics and Astronautics
Stanford University
Stanford, California

for

U. S. ARMY AVIATION MATERIEL LABORATORIES
FORT EUSTIS, VIRGINIA

ABSTRACT

The maximum strength of initially imperfect, axially compressed, circular cylindrical shells has been studied with the use of Reissner's variational principle, von Kármán-Donnell shell theory, and a deformation theory of plasticity. The results of the present analysis reflect families of load-end shortening curves for long circular cylinders. For a given material, each curve relates not only to an imperfection parameter which provides a loading path into the inelastic range but also to the radius-to-wall thickness ratio. Significant maximum strength reductions are obtained, relative to predictions based on linear-elastic theory, for specific materials in the range of radius-to-thickness ratios of practical interest.

TABLE OF CONTENTS

LIST OF ILLUSTRATIONS

LIST OF SYMBOLS

A	Area of cross section, $in.^2$
A_{ij}	Direct stress parameters
a_T	Total radial displacement amplitude of the arch and beam-arch analog, in.
a	Radial displacement amplitude of the arch and beam-arch analog, in.
a_o	Initial deviation in the radial direction of the arch and beam-arch analog, in.
a_{ij}, b_{ij} c_{ij}, d_{ij}	Bending stress parameters
E	Young's modulus, psi
E_s	Secant modulus, psi
e	Unit end shortening, in./in.
e_{cl}	Classical unit end shortening, in./in.
F'	Stress energy density, psi
F_{ij}, H_{ij}	Strain parameters, in./in.
h	Thickness of a two-element cylinder or beam, in.
i,j	Integers
K	Ramberg-Osgood material constant
L	Length of cylinder or beam, in.
M_x, M_y	Bending moments per unit length, lb
M_{xy}	Twisting moment per unit length, lb
m	Number of axial waves
N	Number of circumferential waves
n	Ramberg-Osgood material constant
p	Uniform load, lbs/in.
R	Radius of circular cylindrical shell, in.

t	Thickness of conventional cylinder, in.
t_f	Thickness of one face of a two-element cylinder or beam, in.
U'',V''	Reissner functionals, lb-in.
u,v,w	Displacement of point on middle surface of cylinder in x-, y-, and z-directions, respectively, in.
V	Volume of body, $in.^3$
w_o	Initial deviation of midsurface displacement in radial direction, in.
w_T	Total midsurface displacement in the radial direction, in.
x,y,z	Cylinder coordinates, in.
γ_{xy}	Total shear strain in xy-plane, in./in.
γ'_{xy}	Shearing strain at middle surface, in./in.
γ''_{xy}	Shearing strain due to twisting, in./in.
Δ	Nondimensional imperfection parameter ($\Delta = \xi_{11_o}/t$)
δ_o	Nondimensional imperfection parameter ($\delta_o = \xi_{11_o}/h$)
ϵ_{eff}	Effective strain, in./in.
ϵ_x,ϵ_y	Total components of strain in x- and y-directions, respectively, in./in.
ϵ'_x,ϵ'_y	Components of strain at middle surface in x- and y-directions, respectively, in./in.
$\epsilon''_x,\epsilon''_y$	Components of strain due to bending in x- and y-directions, respectively, in./in.
η	Circumferential wave parameter in conventional cylinder
κ_x,κ_y	Changes in curvature of the shell midsurface, 1/in.
κ_{xy}	Change in twist of shell midsurface, 1/in.
λ_B,λ_A	Wave lengths in axial and circumferential directions, respectively, of beam-arch analog, in.
λ_x,λ_y	Buckle half wave lengths in axial and circumferential directions, respectively, in.

μ	Buckle aspect ratio
ν	Poisson's ratio
ξ	Displacement parameter of the beam-arch analog
ξ_{ij}	Displacement parameters
ξ_{ij_o}	Nondimensional imperfection waveform parameters
ρ	Radius of curvature of the arch
σ	Average compressive stress, psi
σ_{cl}	Classical buckling stress, psi
σ_A	Direct stress coefficient of the arch, psi
σ_{eff}	Effective stress, psi
σ_x, σ_y	Components of direct stress in x- and y-directions, respectively, psi
σ'_x, σ'_y	Local average direct stress in x- and y-directions, respectively, psi
σ''_x, σ''_y	Bending stress in x- and y-directions, respectively, psi
$\sigma_1 \sigma_{1A}$	Bending stress coefficients of the beam-arch analog, psi
τ_{xy}	Total shear stress in xy-plane, psi
τ'_{xy}	Local average shear stress, psi
τ''_{xy}	Shear stress due to twisting, psi

SUBSCRIPTS

b	Refers to the bottom face of the two-element cylinder
f	Refers to the face sheets of the two-element cylinder
i,j	Integers
o	Refers to a radial initial imperfection shape
T	Refers to total displacement
t	Refers to the top face of the two-element cylinder
x,y	Refers to x- and y-directions, respectively

INTRODUCTION

For almost forty years, many investigators have attempted to resolve the discrepancy between classical theory and experiment for thin circular cylindrical shells subjected to uniform axial compression. Within the last several years, three comprehensive survey papers on shell buckling have been prepared by Hoff[1,2] and Stein[3], with the strongest emphasis directed to thin-walled, circular cylindrical shells in axial compression. Both survey authors attribute the discrepancy between the theory and experiment to the combined effects, in varying degrees, of prebuckling deformations, initial imperfections, and boundary conditions; yet, except for noting the possible limitation of linear elastic theory, the quantitative effect of inelastic deformations on the initial buckling (maximum) strength of such shells is neither discussed nor estimated by either of the authors on the basis of the literature surveyed. However, in view of the experimental work of a number of investigators directed to initially imperfect, axially compressed, circular cylindrical shells (see refs. 4,5,6, and 7), not only have inelastic deformations been detected at buckling (maximum load) but they have been shown to reduce the load-carrying capacity significantly as a result. Further, several approximate analyses (refs. 4,7,8, and 9) have indicated the presence of inelastic deformations at initial buckling of imperfect shells. (The inelastic buckling of imperfect shells investigated by Lee[10] is noted here but not discussed further, as interest is being centered on shells which, in the absence of imperfections, would buckle only in the elastic range.) Since the circular cylindrical shell is a basic structural element in aerospace design and since its initial buckling load is indeed its maximum load, a clear understanding of <u>all</u> of the factors influencing its initial or maximum load under axial compression and the relative magnitudes of these factors is necessary.

Now, in the case of plates compressed beyond the classical buckling load, it is well known that a <u>unique</u> load-shortening curve exists for all plates of a given material independent of width-to-thickness ratio, as long as the material follows a linear-elastic, stress-strain law. However, a series of analyses by Mayers et al.[11,12,13], leading to an essentially exact solution for the maximum strength of compressed rectangular plates, based upon

von Kármán's large-deflection, strain-displacement relations, has shown that every plate of a given material, but different width-to-thickness ratio, compressed beyond the classical buckling load into the inelastic range, possesses a unique load-end shortening curve and, hence, maximum load. Similarly, existing von Kármán-Donnell-type elastic postbuckling analyses of axially compressed, long, thin cylinders indicate again a unique load-shortening relationship for all radius-to-thickness ratios. Now, as a result of the present study, families of load-shortening curves have been obtained for initially imperfect, long circular cylinders. Each curve for a given material relates to a particular value of the radius-to-wall thickness ratio and to an initial imperfection pattern which provides a loading path into the inelastic range, since the classical buckling load for compressed cylinders, unlike plates, is never reached in reality. In the range of radius-to-thickness ratios of practical interest for both unstiffened and stiffened shells, significant maximum strength reductions are obtained relative to predictions based on any theory utilizing linear stress-strain behavior.

The maximum strength behavior of initially imperfect, axially compressed, circular cylindrical shells has been studied with the use of a modified form of Reissner's variational principle[14] and the von Kármán-Donnell strain displacement relations. In general, Reissner's variational principle not only permits the selection of the stresses independent of the displacements but also facilitates the incorporation of inelastic effects into the analysis. Confidence in the inelastic analysis based on Reissner's principle has been established herein by comparing the special case of the purely elastic solution with that obtained by Kempner[15] through the use of the minimum total potential energy principle. A similar procedure was followed with respect to plates in the analyses of reference 13. With confidence thus established in the method of solution, inelastic, maximum strength, radius-to-thickness-dependent, load-shortening curves have been obtained for shells of different materials. To obtain the present maximum strength criteria for thin shells, the problem is investigated qualitatively and economically by using a beam-arch analog for the cylinder and quantitatively by analyzing the circular cylindrical shell on the basis of analog-generated trends.

GENERAL THEORY

STATEMENT OF THE PROBLEM AND BASIC ASSUMPTIONS

The problem considered is that of the maximum strength analysis of a long, initially imperfect, circular cylindrical shell. The solution for the shell maximum strength is obtained through the use of Reissner's variational principle modified to include the effects of nonlinear-elastic material behavior. No unloading in the nonlinear-elastic range is assumed to occur; thus, the terms nonlinear-elastic and inelastic are used interchangeably. The presence of unloading in the plastic range is investigated a posteriori, and the effect of unloading, if any, on the solution obtained is assessed in the discussion of the results of the analysis. To establish confidence in the inelastic analysis, the elastic solution for the postbuckling problem is extracted and compared with that developed on the basis of the minimum total potential energy principle.

As in the plate analyses of references 11-13, a two-element description of the shell cross section (Figure 1) is used to avoid the complexity, due to inelastic effects, of integrating a nonlinear stress distribution through the cylinder wall. The core separating the two elements is assumed to be rigid in shear, and the inelastic behavior (constitutive equations and yield criterion) is based upon simple deformation theory. Material compressibility effects in the inelastic analysis are assumed to be negligible; therefore, Poisson's ratio is taken as one-half whenever the load-shortening relationship reflects nonlinear behavior.

The von Kármán-Donnell strain-displacement equations for an initially imperfect, thin-walled, circular cylindrical shell are used in the present analysis. For the radial deflection-thickness ratio magnitudes involved in an initial buckling or maximum strength analysis of a thin shell in compression, and in view of the findings of Mayers and Rehfield[9] based on a more accurate nonlinear theory for thin shells, the use of the von Kármán-Donnell strain-displacement relations is deemed justified.

BASIC EQUATIONS

The von Kármán-Donnell strain-displacement relations for the circular cylindrical shell are modified to include the effect of initial imperfections. Initial imperfections, as defined herein, are deviations from the exact circular cylindrical shape of the shell which are present before any axial compression takes place.

The total displacements of the shell can be expressed as

$$\begin{aligned} u_T &= u \\ v_T &= v \\ w_T &= w_o + w \end{aligned} \tag{1}$$

where w_o is the initial radial deviation of the shell from its exact shape and u, v, and w (see Figure 1) are the additional displacements of the shell from the initial shape during the loading process. The mid-surface strain-displacement equations in terms of total displacements are

$$\begin{aligned} \epsilon'_x &= u_{,x} + \frac{1}{2}(w_{T,x}^2 - w_{o,x}^2) \\ \epsilon'_y &= v_{,y} + \frac{1}{2}(w_{T,y}^2 - w_{o,y}^2) - \frac{(w_T - w_o)}{R} \\ \gamma'_{xy} &= u_{,y} + v_{,x} + w_{T,x}w_{T,y} - w_{o,x}w_{o,y} \end{aligned} \tag{2}$$

The curvature-displacement equations are

$$\begin{aligned} \kappa_x &= -w_{T,xx} + w_{o,xx} \\ \kappa_y &= -w_{T,yy} + w_{o,yy} \\ \kappa_{xy} &= -w_{T,xy} + w_{o,xy} \end{aligned} \tag{3}$$

The total strains are given by

$$\begin{aligned} \epsilon_x &= \epsilon'_x + z\kappa_x \\ \epsilon_y &= \epsilon'_y + z\kappa_y \\ \gamma_{xy} &= \gamma'_{xy} + 2z\kappa_{xy} \end{aligned} \tag{4}$$

VARIATIONAL PRINCIPLE

The Reissner variational principle for prescribed surface displacement

(shell under controlled end-shortening) selects from among all states of stress and displacement which satisfy the boundary conditions of prescribed surface displacement, the true state of stress and displacement by requiring the satisfaction of the equation

$$\delta U = \delta\left\{\iiint_V (\sigma_x \epsilon_x + \sigma_y \epsilon_y + \tau_{xy}\gamma_{xy} - F')dV\right\} = 0 \tag{5}$$

where the stress and displacement states are varied independently. F', the stress energy density, is a function of the stresses such that the stresses and strains are related by the constitutive equations

$$\epsilon_x = \frac{\partial F'}{\partial \sigma_x} \qquad \epsilon_y = \frac{\partial F'}{\partial \sigma_y} \qquad \gamma_{xy} = \frac{\partial F'}{\partial \tau_{xy}} \tag{6}$$

For linear problems, F' becomes the complementary energy density. The principle establishes the Euler equations, which consist of three equilibrium equations and three stress-displacement relations, as well as the associated boundary integrals from which natural boundary conditions, if any, can be established. The Euler equations and boundary conditions for the circular cylindrical shell behaving according to the von Kármán-Donnell theory are developed in Appendix I.

The stress energy density F' is defined, in general, as

$$F' = \int_0^{\sigma_x} \epsilon_x d\sigma_x + \int_0^{\sigma_y} \epsilon_y d\sigma_y + \int_0^{\tau_{xy}} \gamma_{xy} d\tau_{xy} \tag{7}$$

From the secant-modulus deformation theory of plasticity, for an incompressible material, the "effective" strain can be written as

$$\epsilon_{eff} = \frac{2}{\sqrt{3}} \sqrt{\epsilon_x^2 + \epsilon_y^2 + \epsilon_x \epsilon_y + \frac{\gamma_{xy}^2}{4}} \tag{8}$$

and "effective" stress as

$$\sigma_{eff} = \sqrt{\sigma_x^2 + \sigma_y^2 - \sigma_x \sigma_y + 3\tau_{xy}^2} \tag{9}$$

where

$$\sigma_{eff} = E_s \epsilon_{eff}$$

and E_s is the secant modulus of the uniaxial stress-strain curve of the material. For the present analysis, the uniaxial-stress strain curves in tension and compression are taken as identical. Based upon equation (7), the incremental form of F' can be written as

$$dF' = \epsilon_x d\sigma_x + \epsilon_y d\sigma_y + \gamma_{xy} d\tau_{xy} \tag{10}$$

As shown in reference 11, the incremental quantity dF' can be expressed also in the form

$$dF' = \epsilon_{eff} d\sigma_{eff} \tag{11}$$

Therefore,

$$F' = \int_0^{\sigma_{eff}} \epsilon_{eff} d\sigma_{eff} \tag{12}$$

The Reissner functional is then expressed as

$$U'' = \iiint_V (\sigma_x \epsilon_x + \sigma_y \epsilon_y + \tau_{xy} \gamma_{xy} - \int_0^{\sigma_{eff}} \epsilon_{eff} d\sigma_{eff}) dV \tag{13}$$

With the introduction of the Ramberg-Osgood[16] three-parameter representation of a uniaxial stress-strain curve in the form

$$\epsilon_{eff} = \frac{\sigma_{eff}}{E} + K \left(\frac{\sigma_{eff}}{E} \right)^n \tag{14}$$

the functional U" becomes

$$U'' = \iiint_V \left\{ \sigma_x \epsilon_x + \sigma_y \epsilon_y + \tau_{xy} \gamma_{xy} - \left[\frac{\sigma_{eff}^2}{2E} + \frac{KE}{n+1} \left(\frac{\sigma_{eff}}{E} \right)^{n+1} \right] \right\} dV \tag{15}$$

Consistent with the two-element description of the shell and after integration over the thickness h, the result, as developed in Appendix I, is

$$\frac{U''}{VE} = \int_0^1 \int_0^1 \left\{ \left(\frac{\sigma'_x}{E}\right) \epsilon'_x + \left(\frac{\sigma'_y}{E}\right) \epsilon'_y + \left(\frac{\tau'_{xy}}{E}\right) \gamma'_{xy} \right.$$

$$+ \left(\frac{\sigma''_x}{E}\right) \epsilon''_x + \left(\frac{\sigma''_y}{E}\right) \epsilon''_y + \left(\frac{\tau''_{xy}}{E}\right) \gamma''_{xy} - \frac{1}{2}\left[\frac{1}{2}\left(\frac{\sigma_{eff}}{E}\right)^2 + \frac{K}{n+1}\left(\frac{\sigma_{eff}}{E}\right)^{n+1}\right]_t$$

$$\left. - \frac{1}{2}\left[\frac{1}{2}\left(\frac{\sigma_{eff}}{E}\right)^2 + \frac{K}{n+1}\left(\frac{\sigma_{eff}}{E}\right)^{n+1}\right]_b \right\} d\omega d\epsilon \qquad (16)$$

where $\omega = x/L$, $\epsilon = y/2\pi R$, and $V = 4\pi t_f LR$.

The total stresses and strains are written in terms of midsurface and bending contributions, as denoted by the primed and double-primed quantities. The subscript t refers to the top face and the subscript b refers to the bottom face of the two-element cross section. With the von Kármán-Donnell strain-displacement equations and the relations for the effective stress in terms of the primed and double-primed quantities, as expressed in reference 13, the Reissner functional becomes

$$\frac{U}{VE} = \int_0^1 \int_0^1 \left\{ \frac{\sigma'_x}{E}[u_{,x} + \frac{1}{2}(w_{T,x}^2 - w_{o,x}^2)] \right.$$

$$+ \frac{\sigma'_y}{E}\left[v_{,y} + \frac{1}{2}(w_{T,y}^2 - w_{o,y}^2) - \frac{(w_T - w_o)}{R}\right]$$

$$+ \frac{\tau'_{xy}}{E}[v_{,x} + u_{,y} + w_{T,x}w_{T,y} - w_{o,x}w_{o,y}]$$

$$+ \frac{\sigma''_x}{E}[\frac{h}{2} w_{,xx}] + \frac{\sigma''_y}{E}[\frac{h}{2} w_{,yy}] + \frac{\tau''_{xy}}{E}[hw_{,xy}]$$

$$- \frac{1}{2}\left[\left(\frac{\sigma'_x}{E}\right)^2 + \left(\frac{\sigma'_y}{E}\right)^2 - \frac{\sigma'_x}{E}\frac{\sigma'_y}{E} + 3\left(\frac{\tau'_{xy}}{E}\right)^2 \right.$$

$$\left. + \left(\frac{\sigma''_x}{E}\right)^2 + \left(\frac{\sigma''_y}{E}\right)^2 - \frac{\sigma''_x}{E}\frac{\sigma''_y}{E} + 3\left(\frac{\tau''_{xy}}{E}\right)^2\right]$$

$$\left. - \frac{1}{2}\frac{K}{(n+1)}\left[\left(\frac{\sigma_{eff}}{E}\right)_t^{n+1} + \left(\frac{\sigma_{eff}}{E}\right)_b^{n+1}\right] \right\} d\omega d\epsilon \qquad (17)$$

In consideration of the linear-elastic problem for a homogeneous cylinder, and with the bending stresses related to the curvatures through Hooke's law, a modified Reissner function (following ref. 13) is expressed in the form

$$\frac{U''}{VE} = \int_0^1\int_0^1 \left\{ \frac{\sigma'_x}{E}\left[u_{,x} + \frac{1}{2}(w_{T,x}^2 - w_{o,w}^2)\right] \right.$$

$$+ \frac{\sigma'_y}{E}\left[v_{,y} + \frac{1}{2}(w_{T,y}^2 - w_{o,y}^2) - \frac{(w_T - w_o)}{R}\right]$$

$$+ \frac{\tau'_{xy}}{E}[v_{,x} + u_{,y} + w_{T,x}w_{T,y} - w_{o,x}w_{o,y}]$$

$$- \frac{1}{2}\left[\left(\frac{\sigma'_x}{E}\right)^2 + \left(\frac{\sigma'_y}{E}\right)^2 - 2\nu\left(\frac{\sigma'_x}{E}\right)\left(\frac{\sigma'_y}{E}\right) + 2(1+\nu)\left(\frac{\tau'_{xy}}{E}\right)^2\right]$$

$$\left. + \frac{t^3}{24(1-\nu^2)}\left[w_{,xx}^2 + w_{,yy}^2 + 2\nu w_{,xx}w_{,yy} + 2(1-\nu)w_{,xy}^2\right]\right\} dx\,dy \qquad (18)$$

This modified form of Reissner's principle leaves only the displacements and midsurface stresses as the variational quantities. As described in the next section, equation (18) is used as the basis of correlation with Kempner's minimum potential energy solution (ref. 15) for the postbuckling load-shortening curve.

METHOD OF SOLUTION

Previous investigators (Cox[17], Tsien[18], and Hoff[19]) have approximated the postbuckling behavior of both axially compressed and uniformly heated, circular cylindrical shells by analyzing various one-dimensional models. These models consist of a basic beam member supported by one or more springs whose load-deflection curves are chosen such as to force the models' load-shortening curves to provide the snap-through behavior associated with the postbuckling behavior of thin shells in compression.

In the present analysis, a model consisting of a beam resting on a series of shallow sinusoidally curved arches, as shown in Figure 2, is selected

to be the analog of the shell. The behavior of an arch under radial loading, shown in Figure 3, provides a nonlinear foundation for the beam so as to yield the snap-through behavior associated with axially compressed, cylindrical shells. The beam length is equivalent to the cylinder length; the arch length is taken as a circumferential wave length of one buckle. The spacing between arches is equivalent to the axial wave length of one buckle of the cylinder. The radius R of the cylinder is brought into the analog geometry through the rise parameter for circularly curved plates of small chord; that is, the maximum rise a_o of the sinusoidally curved arch in Figure 3 is equated to the rise of a shallow, circularly curved plate through the relationship $a_o = \lambda_A^2/8R$.

SHALLOW ARCH BEHAVIOR

A Reissner functional for a shallow arch subjected to a prescribed uniform loading is

$$\frac{U_A'' + V_A''}{EA} = \int_0^{\lambda_A} \left\{ \frac{\sigma_y'}{E} \left[v_{,y} + \frac{1}{2} w_{,y}^2 - \frac{w}{\rho} \right] + \frac{\sigma_y''}{E} \left[\frac{h}{2} w_{,yy} \right] - \frac{1}{2} \left[\left(\frac{\sigma_y'}{E} \right)^2 + \frac{1}{3} \left(\frac{\sigma_y''}{E} \right)^2 \right] \right\} dy - \frac{p}{E} \int_0^{\lambda_A} w dy \qquad (19)$$

where V'' = potential of the prescribed loading

$\frac{1}{\rho}$ = variable curvature = $- w_{o,yy}$

w_o = initial shape

p = uniform load

DISPLACEMENT AND STRESS FORMULATIONS

Functions for the displacements and stresses are chosen in the form

$$\frac{w_o}{h} = \frac{a_o}{h} \sin \frac{\pi y}{\lambda_A}$$

$$\frac{w}{h} = \frac{a}{h} \sin \frac{\pi y}{\lambda_A}$$

$$v = 0$$

$$\frac{\sigma'_y}{E} = \frac{\sigma_A}{E}$$

$$\frac{\sigma''_y}{E} = \frac{\sigma_{1A}}{E} \sin \frac{\pi y}{\lambda_A} \tag{20}$$

The use of a vanishing v-displacement in conjunction with the modified-Reissner-principle approach and the von Kármán strain- displacement equations has been justified in reference 13 for plates. For the arch, with the kinematics described by a specialization of the von Kármán-Donnell curved plate equations, the stresses and w displacement can be determined from the first variation of the Reissner functional regardless of the Fourier-series representation for v. Thus, in the absence of any possible coupling of σ_y and v in the strain energy, it is obvious that v can be equated to zero without any loss in generality.

LOAD-DEFLECTION CURVE

Substitution of equation (20) into equation (19), with subsequent integration over the arch length and variation with respect to the amplitudes of the displacements and stresses, results in three simultaneous equations for the determination of the nondimensionalized displacement and stress parameters for a, σ_A, and σ_{1A} defined in equation (20). The simultaneous equations can be written conveniently in terms of only one of the parameters (equation (60) of Appendix II); that is,

$$\xi^3 - \frac{3\pi^2}{2\eta}\xi^2 + \left(\frac{\pi^4}{2\eta^2} + \frac{1}{3}\right)\xi = \left(\frac{16}{\eta}\right)^2 \frac{\bar{p}}{\pi} \tag{21}$$

where

$$\xi = a/h$$

$$\eta = \frac{\pi^2}{2}\frac{h}{a_o}$$

$$\bar{p} = \frac{ph}{EA}\left(\frac{R}{h}\right)^2$$

A plot of $\bar{p}$ vs. ξ is shown in Figure 3.

It is interesting to note that the single variationally derived equation above, for the case of a linear-elastic constitutive law (Hooke's law), reproduces exactly the load-deflection curve for a shallow arch constructed by Timoshenko[20] from two equations derived from beam theory with midplane stretching effects included.

BEAM-ARCH ANALOG

The Reissner functional for the entire beam-arch model, including the effects of inelastic behavior and the use of the two-element description for the beam and arch cross sections, is written as

$$\frac{U_A'' + U_B''}{VE} = \int_0^1 \left\{ \frac{\sigma_x'}{E}\left[u_{,x} + \frac{1}{2} w_{,x}^2 + w_{,x} w_{o,x} \right] + \frac{\sigma_x''}{E}\left[\frac{h}{2} w_{,xx} \right] - \frac{1}{2}\left[\left(\frac{\sigma_x'}{E} \right)^2 + \left(\frac{\sigma_x''}{E} \right)^2 \right] - \frac{K}{2(n+1)}\left[\left(\frac{\sigma_{xeff}}{E} \right)_t^{n+1} + \left(\frac{\sigma_{xeff}}{E} \right)_b^{n+1} \right] \right\} d\omega$$

$$+ \int_0^1 \left\{ \frac{\sigma_y'}{E}\left[v_{,y} + \frac{1}{2} w_{,y}^2 - \frac{w}{|\rho|} \right] + \frac{\sigma_y''}{E}\left[\frac{h}{2} w_{,yy} \right] - \frac{1}{2}\left[\left(\frac{\sigma_y'}{E} \right)^2 + \left(\frac{\sigma_y''}{E} \right)^2 \right] - \frac{K}{2(n+1)}\left[\left(\frac{\sigma_{yeff}}{E} \right)_t^{n+1} + \left(\frac{\sigma_{yeff}}{E} \right)_b^{n+1} \right] \right\} d\varphi \qquad (22)$$

where $\varphi = y/\lambda_A$, $\omega = x/\lambda_B$.

DISPLACEMENT AND STRESS FORMULATIONS

In addition to equation (20), expressions for the beam displacement and stresses are

$$u = -ex$$

$$\frac{\sigma_x'}{E} = -\frac{\sigma}{E}$$

$$\frac{\sigma''_x}{E} = \frac{\sigma_1}{E} \sin \frac{\pi x}{\lambda_B} \tag{23}$$

where e = prescribed end shortening. The use of midsurface displacements involving no free parameters in conjunction with the modified-Reissner-principle approach has been justified for plates and shells in references 9 and 13 and is demonstrated herein for the arch. Thus, the stresses and w displacement can be determined from the first variation of the Reissner functional regardless of any additional Fourier-series representation for u; therefore, it is sufficient to describe u as -ex.

LOAD-SHORTENING RELATIONSHIP (ELASTIC PROBLEM)

For elastic behavior, K is set equal to zero in equation (22). As shown in Appendix II, substitution of equations (20) and (23) for the assumed stresses and displacements of the arch and beam, respectively, into the total Reissner functional (eq. (22)) for the analog, followed by integration over one wave length in each direction and variation with respect to all free parameters, leads to five simultaneous equations which can be reduced by elimination to only two equations; that is,

$$\frac{\sigma R}{Eh} = \frac{eR}{h} - \frac{\mu^2 \eta}{16}[\xi^2 + 2\xi\delta_o] \tag{24}$$

and

$$\xi^3\left[1 + \frac{1}{\mu^4}\right] + \xi^2\left[3\delta_o - \frac{3\pi^2}{2\eta\mu^4}\right] + \xi\left[-\frac{16}{\mu^2\eta}\left(\frac{eR}{h}\right) + 2\left(\delta_o^2 + \frac{\pi^4}{4\eta^2\mu^4}\right) + 1 + \frac{1}{\mu^4}\right] - \frac{16\delta_o}{\mu^2\eta}\left(\frac{eR}{h}\right) = 0 \tag{25}$$

These equations are solved in the following manner. First, for given values of the parameters eR/h, μ, η, and δ_o, equation (25) is evaluated numerically for ξ. Then, for the given parameter values and the corresponding ξ's, equation (24) is solved numerically to establish the relationship between $\sigma R/Eh$ and eR/h; namely, the family of imperfection-dependent load-shortening curves shown in Figure 4.

LOAD-SHORTENING RELATIONSHIP (INELASTIC PROBLEM)

The inelastic behavior is studied by retaining the two terms multiplied by the parameter K in equation (22). To enter the inelastic range, an elastic analysis is repeated at an end-shortening value which insures elastic behavior. The parameter values obtained are utilized as starting points for the inelastic analysis. A Newton-Raphson procedure is employed to establish the load-shortening curves for inelastic behavior with increasing values of the end shortening. Families of radius-to-thickness-dependent, load-shortening curves are then obtained for E, K, and n values corresponding to electroformed nickel (see stress-strain curve in Figure 5). Such load-shortening curves are presented in Figure 6. The thickness t of the homogeneous material is related to the distance separating the two faces of the model by setting the critical load of the two-element shell equal to the critical load of the homogeneous shell of given R/t. The resulting relationship between h and t is simply $h/t = 1/\sqrt{3}$.

CIRCULAR CYLINDRICAL SHELL

DISPLACEMENT AND STRESS FORMULATIONS

The maximum strength of a long, circular cylindrical shell is studied for both the elastic and inelastic problems by enforcing the vanishing of the first variation of functionals given by equations (18) and (17), respectively. The variations are carried out with respect to assumed states of stress and displacement, with the latter being kinematically admissible.

The approach followed is that of prescribing the stresses and the radial deflection pattern in the same form as those formulated by Kempner[15]. After a point on Kempner's elastic postbuckling curve is reproduced by the elastic results of the present analysis (K = 0 in eq. (22)), confidence in the elastic analysis is established. The radial displacement in any one buckle of the shell is selected to be

$$w = h\left(\xi_{00} + \xi_{11}\cos\frac{\pi x}{\lambda_x}\cos\frac{\pi y}{\lambda_y} + \xi_{20}\cos\frac{2\pi x}{\lambda_x} + \xi_{02}\cos\frac{2\pi y}{\lambda_y}\right) \qquad (26)$$

The corresponding midsurface displacements would in general be taken as

$$u = -ex + \sum_{i=1}^{\infty}\sum_{j=1}^{\infty} u_{ij} \sin\frac{i\pi x}{\lambda_x}\cos\frac{j\pi y}{\lambda_y}$$

$$v = \sum_{i=1}^{\infty}\sum_{j=1}^{\infty} v_{ij} \cos\frac{i\pi x}{\lambda_x}\sin\frac{j\pi y}{\lambda_y}$$

However, the use of expressions for u and v involving no free parameters in conjunction with the modified-Reissner-principle approach has been demonstrated in references 9 and 13 and discussed earlier with reference to both the arch and the beam-arch analog. It has been shown that the stresses and radial displacement may be determined from the first variation of the Reissner functional, regardless of the values of u_{ij} and v_{ij}, when the von Kármán-Donnell strain-displacement relations are used along with Fourier-series representations for both displacements and stresses. Thus, it is once more concluded that u_{ij} and v_{ij} can be equated to zero without any loss in generality; the midsurface displacements become simply

$$u = -ex \tag{27}$$

$$v = 0 \tag{28}$$

The rationale underlying the utilization of midsurface displacements reflecting no free parameters in references 9 and 13 as well as the present work is simply the realization that either nonexistent or very weak coupling exists between free midsurface stresses and displacements in a Reissner formulation, depending upon the degree of nonlinearity in the plate or shell kinematics being employed.

The simplification of the expressions for the midsurface displacements involving no free parameters permits the equilibrium equations in the x and y directions to be satisfied independently of the magnitudes of the free stress coefficients.

The inplane stresses, in addition to the average axial stress, consist of the Fourier harmonics found in Kempner's stress function (ref. 15) and are expressed in the form

$$\frac{\sigma'_x}{E} = -\left[\frac{\sigma}{E} + A_{11}\cos\frac{\pi x}{\lambda_x}\cos\frac{\pi y}{\lambda_y} + 4A_{22}\cos\frac{4\pi x}{\lambda_x}\cos\frac{4\pi y}{\lambda_y} + 9A_{13}\cos\frac{\pi x}{\lambda_x}\cdot\right.$$

$$\left.\cos\frac{3\pi y}{\lambda_y} + A_{31}\cos\frac{3\pi x}{\lambda_x}\cos\frac{\pi y}{\lambda_y} + 4A_{02}\cos\frac{2\pi y}{\lambda_y}\right] \qquad (29)$$

$$\frac{\tau'_{xy}}{E} = -\mu\left[A_{11}\sin\frac{\pi x}{\lambda_x}\sin\frac{\pi y}{\lambda_y} + 4A_{22}\sin\frac{2\pi x}{\lambda_x}\sin\frac{2\pi y}{\lambda_y} + 3A_{13}\sin\frac{\pi x}{\lambda_x}\cdot\right.$$

$$\left.\sin\frac{3\pi y}{\lambda_y} + 3A_{31}\sin\frac{3\pi x}{\lambda_x}\sin\frac{\pi y}{\lambda_x}\right] \qquad (30)$$

$$\frac{\sigma'_y}{E} = -\mu^2\left[A_{11}\cos\frac{\pi x}{\lambda_x}\cos\frac{\pi y}{\lambda_y} + 4A_{22}\cos\frac{2\pi x}{\lambda_x}\cos\frac{2\pi y}{\lambda_y} + A_{13}\cos\frac{\pi x}{\lambda_x}\cos\frac{3\pi y}{\lambda_y}\right.$$

$$\left. + 9A_{31}\cos\frac{3\pi x}{\lambda_y}\cos\frac{\pi y}{\lambda_y} + 4A_{20}\cos\frac{2\pi x}{\lambda_x}\right] \qquad (31)$$

It is noted that the variable coefficients in σ'_x/E, τ'_{xy}/E, and σ'_y/E are the same. This equivalence is established automatically from the satisfaction of the inplane equilibrium equations in the x- and y-directions, respectively, prior to employing the variational principle, because the displacements u and v in equations (27) and (28) are not arbitrary.

Now, instead of relating the bending stresses to the curvatures through Hooke's law, they are selected in the form of the curvatures, but with arbitrary coefficients, and are written as

$$\frac{\sigma''_x}{E} = a_{11}\cos\frac{\pi x}{\lambda_x}\cos\frac{\pi y}{\lambda_y} + a_{20}\cos\frac{2\pi x}{\lambda_x} + a_{02}\cos\frac{2\pi y}{\lambda_y} \qquad (32)$$

$$\frac{\sigma''_y}{E} = \mu^2\left[b_{11}\cos\frac{\pi x}{\lambda_x}\cos\frac{\pi y}{\lambda_y} + b_{20}\cos\frac{2\pi x}{\lambda_x} + b_{02}\cos\frac{2\pi y}{\lambda_y}\right] \qquad (33)$$

$$\frac{\tau_{xy}}{E} = \mu\left[d_{11}\sin\frac{\pi x}{\lambda_x}\sin\frac{\pi y}{\pi_y}\right] \qquad (34)$$

The justification for this assumption is established in references 9 and 13 through comparison of results with those of well-known, essentially exact solutions for postbuckling analyses of shells and plates, respectively.

Because of the periodic nature of the assumed expressions for the nonuniform stresses and displacements, the boundary integrals derived on the basis of the Reissner variational principle in Appendix I can be reduced to

$$\int_0^L \sigma_y' dx = 0 \qquad \text{for any } y \tag{35}$$

$$\int_0^L \tau_{xy}' dx = 0 \qquad \text{for any } y \tag{36}$$

$$\frac{1}{2\pi R} \int_0^{2\pi R} \sigma_x' dy = -\sigma \qquad \text{for any } x \tag{37}$$

It can be seen immediately that expressions (29), (30), and (31) for the stresses satisfy the integral conditions (35), (36), and (37).

INITIAL IMPERFECTION PATTERN

In a recent report by Tennyson and Welles[21], the authors note that the first terms to be observed experimentally at the inception of buckling are those described by the combination of an asymmetric plus an axisymmetric term. Moreover, from their analysis of free vibrations of thin-walled cylinders, Mayers and Wrenn[22] point out that for finite displacements of the order of magnitude of the shell thickness, the minimum energy is related to a slightly "modified-chessboard" radial deflection pattern given by the same harmonics as those in reference 21. It is conjectured, therefore, that in view of the random nature of imperfections in thin shells, a reasonable imperfection shape to which the shell might be particularly sensitive is

$$w_o = h\left[\xi_{11_o} \cos\frac{\pi x}{\lambda_x} \cos\frac{\pi y}{\lambda_y} + \xi_{20_o} \cos\frac{2\pi x}{\lambda_x}\right] \tag{38}$$

LOAD-SHORTENING RELATIONSHIP (ELASTIC PROBLEM)

To establish the all-elastic, load-shortening curves for the circular cylindrical shell, a stationary value of the Reissner functional U" with respect to the free parameters ξ_{ij}, A_{ij}, and σ/E is sought (see Appendix

III). The set of equations established from the vanishing of the first variation is reducible to four equations in the four unknowns σ/E, ξ_{11}, ξ_{20}, and ξ_{02}. This set of four equations is then used to construct the imperfection-dependent, elastic load-shortening curves presented in Figure 7 for $\mu = 1$ and $\eta = 0.45$. These equations are used also to reproduce a point on the Kempner load-shortening curve for $\mu = 0.3899$, $\eta = 0.226$, $eR/t = 0.4$, and $\Delta = 0.0$ as a means of establishing the accuracy of the analysis.

LOAD-SHORTENING RELATIONSHIP (INELASTIC PROBLEM)

In the inelastic problem, the load-shortening curve for the circular cylindrical shell is obtained by finding the extrema of the following functional:

$$\frac{U''}{VE} = \frac{U''}{VE}\text{ elastic} - \frac{1}{2}\frac{K}{(n+1)}\int_0^1\int_0^1\left[\left(\frac{\sigma_{eff}}{E}\right)_t^{n+1} + \left(\frac{\sigma_{eff}}{E}\right)_b^{n+1}\right]d\alpha d\epsilon \qquad (39)$$

which consists initially of 17 free parameters.

The additional free parameters over the four required for the elastic solution appear because the bending stresses, even though taken in the form of the curvatures, require seven additional free parameters when the deflection function is as given by equation (26); further, the six mid-surface stress components, A_{ij}, cannot be eliminated in terms of the ξ_{ij} and σ/E because the inelastic contribution to the total Reissner functional, which contains the ξ_{ij} and σ/E, requires that the extrema of equation (39) be found numerically. As a result, equation (39) is written in terms of the 17 free parameters $\xi_1,\xi_2,\xi_3,A_{11},A_{22},A_{13},A_{13},A_{02}$, $A_{20},a_{11},a_{20},a_{02},b_{11},b_{20},b_{02},d_{11}$, and σ/E. The double integral in equation (39) is evaluated numerically by a Newton-Raphson iteration technique, and maximum-strength, radius-to-thickness-dependent, load-shortening curves are obtained for three kinds of materials: 2024-T3 aluminum, electroformed nickel, and electroformed copper. Except for the radius-to-thickness ratio, the parameter values used are the same as those taken for the elastic analysis which is applicable to all values of R/t. A

unique load-shortening curve (independent of R/t) for all-elastic analyses is typical of solutions based on the von Kármán theory for plates and the von Kármán-Donnell theory for shells (see, for example, refs. 1, 2, 3, and 13).

RESULTS AND DISCUSSION

The maximum strength of initially imperfect, axially compressed, circular cylindrical shells has been studied through the use of modified forms of Reissner's variational principle, in conjunction with the von Kármán-Donnell theory and a deformation theory of plasticity. Maximum-strength, radius-to-thickness-dependent, load-shortening curves have been obtained for three different materials, utilizing both a beam-arch analog to represent the cylinder and a two-dimensional analysis of the circular cylindrical shell itself. The fundamental materials considered are nickel and copper, in view of the fact that most of the experimental work carried out in recent years to study imperfection sensitivity relative to axial compression loading of carefully manufactured (electroformed) shells has dealt with these materials. Results are presented also for 2024-T3 aluminum shells, since design practice reflects such a more conventional material.

BEAM-ARCH ANALOG

With the use of the beam-arch analog, maximum-strength, radius-to-thickness-dependent, load-shortening curves have been obtained that represent cylinders with material properties corresponding to electroformed nickel. For a given imperfection amplitude, the load-shortening curves for electroformed nickel reflect a radius-to-thickness dependence of significant magnitude, as depicted graphically in Figure 6. The upper curve represents the results of an all-elastic analysis. The family of curves below the purely elastic-analysis curve is obtained by incorporating inelastic effects into the variational principle, using the stress-strain curve of Figure 5 and perturbing from the original elastic-solution parameters established in developing the all-elastic behavior curve. It is noted that for $R/t = 300$ and $\Delta = 0.1$, the reduction in maximum load from the maximum load obtained in the purely elastic analysis is 16%. Also, for this arbitrary case, it may be seen that for a sufficiently "thin" shell, say, $R/t > 1000$, the

inelastic analysis reflects the absence of inelastic strains and coalesces with the unique elastic analysis result (all R/t).

CIRCULAR CYLINDRICAL SHELL

For circular cylindrical shells, maximum-strength, radius-to-thickness dependent, load-shortening curves have been obtained utilizing stress-strain curves representing several different materials. The survey papers of Hoff[1,2] and Stein[3] indicate that a number of investigators have achieved unusually high buckling stresses relative to the classical stress by performing exacting experiments on very carefully fabricated specimens. The results of these investigators are included in Figure 8, along with a band encompassing the myriad tests performed prior to 1960. The source of the band is an indication of the significant discrepancy and scatter that existed between experiment and classical theory over a period of about 30 years.

Above the upper bound of the scatter band, results are shown for the very specialized tests carried out by Babcock and Sechler[23], Horton and Durham[5], Tennyson and Welles[21], and Almroth et al.[24] The Babcock and Sechler tests were performed on electroformed copper cylinders, the Horton et al. and Almroth et al. tests were performed on electroformed nickel cylinders, and the Tennyson and Welles tests were performed on a series of spun-cast plastic cylinders. In each instance, relatively small cylinders were involved, and the control of any irregularities in the shell geometries is obvious due to the fact that the classical load is approached within 10 percent on one end (R/t = 100) and 25 percent on the other (R/t = 1000), which is well above the upper bound of the scatter band for much larger shells fabricated in accordance with common shop practices over several decades.

From Figure 8, it would appear that the Almroth et al. and Babcock and Sechler electroformed nickel and copper shells are the most imperfection sensitive; thus, these particular materials are of analysis interest. The uniaxial stress-strain curve utilized in the analysis of the electroformed nickel shells has been presented previously as Figure 5, in conjunction with the inelastic beam-arch analog leading to the load-shortening curves shown in Figure 6. Now, with this stress-strain curve, the cylinder analysis yields the load-shortening relationships presented in Figure 9.

The results show that for $\mu = 1$ and $\Delta = 0.1$, the reduction from all-elastic behavior to the $R/t = 300$ cylinder is about 25 percent. It is noted then that (1) inelastic deformations can be present in cylinders which if perfect would buckle at the classical elastic load and that (2) the phenomenon of inelastic deformations produces a significant R/t-dependence of the load-shortening curve for a cylinder of a given material and imperfection parameter.

The family of load-shortening curves shown in Figure 9 is related to only one value of this imperfection parameter. However, for usual allowable design tolerances, imperfections for cylinders corresponding to large radius-to-thickness ratios would be expected to be "effectively" greater than those of cylinders corresponding to relatively small radius-to-thickness ratios. Therefore, the radius-to-thickness ratios are correlated to reasonable imperfection parameters (namely, the average values of the scatter band for practically fabricated shells of Figure 8) to establish the imperfection parameter as a function of R/t; the ensuing load-shortening curves are shown in Figure 10.

Each set of curves for various R/t values in Figure 10 is related to a given imperfection parameter; the imperfection parameter increases as the radius-to-thickness ratio increases. Clearly, as should be expected, cylinders corresponding to large radius-to-thickness ratios (for example, $R/t = 800$) possess lower maximum loads than cylinders of significantly smaller radius-to-thickness ratios (for example, $R/t = 400$). This phenomenon has been demonstrated experimentally by Kanemitsu and Nojima[25] and Weingarten et al.[6] It may be seen from Figures 9 and 10 that as the radius-to-thickness ratio decreases, the effect of inelastic deformations increases. In Figure 10, the load-shortening curves for $R/t = 400$, 600, and 800 depart significantly from the elastic curves for the same imperfection amplitude, ranging from about 8 percent for the thinnest cylinder to 25 percent for the thickest cylinder, which is still relatively thin by design standards. It may be noted also that cylinders of different geometries may exhibit the same maximum load as shown in Figure 10. A cylinder of $R/t = 600$ and $\Delta = 0.1$ has essentially the same maximum load as a very thin cylinder (that is, $R/t > 1000$) and $\Delta = 0.16$. The maximum load

of the first cylinder depends not only on the initial imperfection amplitude but also on local yielding of the material, whereas the maximum load of the second cylinder depends only upon the relatively large imperfection. This is attributed to the fact that bending predominates and prevents the development of membrane strains which are of sufficient magnitude to combine with the bending strains and cause local yielding of the material. As a result, the total effective stress remains well below the yield point of the uniaxial stress-strain curve for the material, and essentially elastic behavior governs.

Now, it is essential to study more closely the actual nickel and copper cylinder tests reported by Almroth et al. and Babcock and Sechler for cylinders of about $R/t = 850$ and 890, respectively. The stress-strain curve for electroformed copper is shown in Figure 11; the corresponding stress-strain curve for electroformed nickel appears in Figure 5. With the fit of the appropriate imperfection parameters, the maximum strengths produced by the cylinder inelastic analysis are shown in Figure 12. The results are obtained on the basis of equal buckle wavelengths ($\mu = 1$) and imperfection amplitudes ($\Delta = 0.02$). When it is assumed that the materials behave in linear elastic fashion, the cylinder analysis predicts maximum strengths some 10-14 percent higher. In other words, the relatively high ratio of σ/σ_{cl} reached in the careful tests on carefully fabricated cylinders could have been higher and closer to the classical theory results reported by Stein[3], had the materials behaved in perfectly elastic fashion.

It is believed that sufficient theoretical evidence has been given, in consideration of the results of the recent experimental references presented, to reach the conclusion that inelastic deformation should not be excluded from initial buckling or maximum strength analyses. However, electroformed nickel and copper are not typical of practical construction materials. Thus, attention is next directed to aluminum, the most common material utilized in aerospace construction. For analysis purpose, the stress-strain curve of 2024-T3 aluminum alloy (Figure 13) is utilized. The resulting load-shortening curves are shown on Figure 14. Surprisingly, the behavior of 2024-T3 aluminum

cylinders in the maximum strength analysis is markedly different from that of the electroformed copper and nickel cylinders. The separation of the load-shortening curves as a function of R/t does not begin until the R/t ratio reaches the neighborhood of 200. In fact, appreciable reduction in maximum strength does not occur until a radius-to-thickness ratio of about 100 is approached. Obviously, there is an effect of the nature of the stress-strain curve on the sensitivity to inelastic effects at a given R/t ratio. Aluminum and other conventional materials exhibit much sharper knees of the stress-strain curve, and this can be noted quickly from the exponent in the Ramberg-Osgood stress-strain curve representation. Whereas the electroformed copper and nickel stress-strain curves reflect exponents of 3, aluminum and most other conventional aerospace metals reflect exponents of 9 or greater. One exception is stainless steel; the uniaxial stress-strain curve is represented quite accurately by an exponent of 3.

Little comfort can be taken from the fact that the 2024-T3 aluminum shells exhibit purely elastic behavior in the range $R/t > 300$. Regardless of choice of conventional structural material, thin shells for resisting compression loads are utilized either in orthotropically stiffened or sandwich forms. As pointed out by Hoff [1], such shells possess "effective" R/t ratios as small as 50. Hence, maximum strength determination for such shells should be based on analyses such as the one described here, which can account for the presence of inelastic deformations. It should be noted that for "effectively" thick shells, initial imperfections would tend to be minimized and the effects of inelastic deformation maximized. In reported compression tests on large design-scale sandwich and orthotropically stiffened shells (refs. 26, 27, 28), in the range $(R/t)_{effective}$, 45-220, maximum calculated stresses indicate inelastic deformations at maximum load. The family of curves presented in Figure 14 illustrates the reduction in maximum load due to plasticity of "effectively" thick compressed shells of 2024-T3 aluminum; the uniaxial stress-strain curve is shown in Figure 13. For $R/t = 60$, the reduction in maximum strength due to inelastic considerations is about 33%. It should be further noted that

the imperfection parameter value ($\Delta = 0.1$) would probably be smaller in practice for shells of effective $R/t \leq 100$; thus, it would be expected that at higher average stress level ratios, σ/σ_{cl}, the percent of reductions in maximum strengths due to inelastic effects should be greater than those shown in Figure 14. A particular curve of interest in Figure 14 is that for $R/t = 167$. This load-shortening curve represents the analytical prediction for a 2024-T3 aluminum test cylinder of NASA (reference 28) with the cross section shown in Figure 14. The imperfection parameter, $\Delta = 0.1$, is taken from the average value of the scatter band of Figure 8 for $R/t = 167$. In this case, little effect of plasticity is seen. However, for $R/t = 167$ and a 2024-T3 stiffened aluminum cylinder, the buckling mode is still representative of thin-cylinder behavior. A photograph of the buckled test cylinder (see Figure 15) clearly shows the "diamond" buckle pattern typical of thin cylinder behavior in the presence of initial imperfections. An efficient stiffened 2024-T3 aluminum cylinder would appear to be one of lower R/t than 167, with resulting smaller imperfection amplitude and increased sensitivity to inelastic deformations.

Finally, for the results obtained herein, based upon a simple deformation theory of plasticity with no unloading mechanism provided, the occurrence of unloading, if any, within a buckle must be assessed. In the case of each shell analyzed, monitoring the numerical calculations for the effective strain at a point, as the end shortening increased incrementally, indicated that no detectable unloading in inelastic regions of a buckle occurred as the maximum load of the shell was approached. Therefore, the initial assumption that the present maximum strength analysis could be undertaken on the basis that the material is of a nonlinear elastic nature was indeed valid.

CONCLUDING REMARKS

The study of the maximum strength of initially imperfect, axially compressed, thin-walled, circular cylindrical shells has been undertaken to determine the effects of inelastic deformations on maximum load-carrying capacity to establish, as was found to be the case of compressed flat plates, the degree of geometry dependence of load-shortening curves for a

given material. Indeed, the load-shortening curves obtained in the present analysis for the inelastic behavior of shells reflect significant radius-to-thickness ratio dependence. A family of load-shortening curves, each corresponding to a different value of radius-to-thickness ratio, is shown to result for a given material and a specific initial imperfection amplitude. The significant spread between the load-shortening curves in any family of such curves is a new result in application of the von Kármán-Donnell strain-displacement relations, which sheds further light on a problem whose satisfactory solution has eluded investigators for decades. The actual solution has been carried out with the use of the von Kármán-Donnell formulation and a deformation theory of plasticity in conjunction with a modified form of the Reissner variational principle.

In view of the results obtained for shells corresponding to experimentally studied electroformed copper and nickel shells of relatively high geometric accuracy, it must be concluded that initial imperfections cannot be considered the only significant cause of such shells' failing to develop their classical buckling stresses. Further, the presence of inelastic deformations and the nature of the nonlinearity of the material stress-strain curve for a given shell cause considerable scatter in maximum strength results for cylinders of the same R/t ratio. Thus, it is reasonable to conclude that inelastic deformations, along with inital imperfections, prebuckling deformations, and boundary conditions (factors previously established to be important), must be considered in determining the maximum strength of thin shells, especially those with small to moderate initial imperfections. Such imperfections would be representative of orthotropically stiffened and sandwich shells in aerospace vehicle designs. The more efficient stiffened or sandwich shell would appear to be one in which elastic buckling would take place except for the presence of some degree of imperfection which precipitates bending with inelastic deformations. These two effects, coupled with prebuckling deformations and boundary conditions, should make optimization procedures more meaningful.

A beam-arch analog developed to represent a circular cylindrical shell

and the shell itself have been used to establish the load shortening curves presented. The analog is introduced to establish qualitative trends and to achieve economy in computation for what must be considered to be an extremely complicated problem in the nonlinear analysis of thin shells.

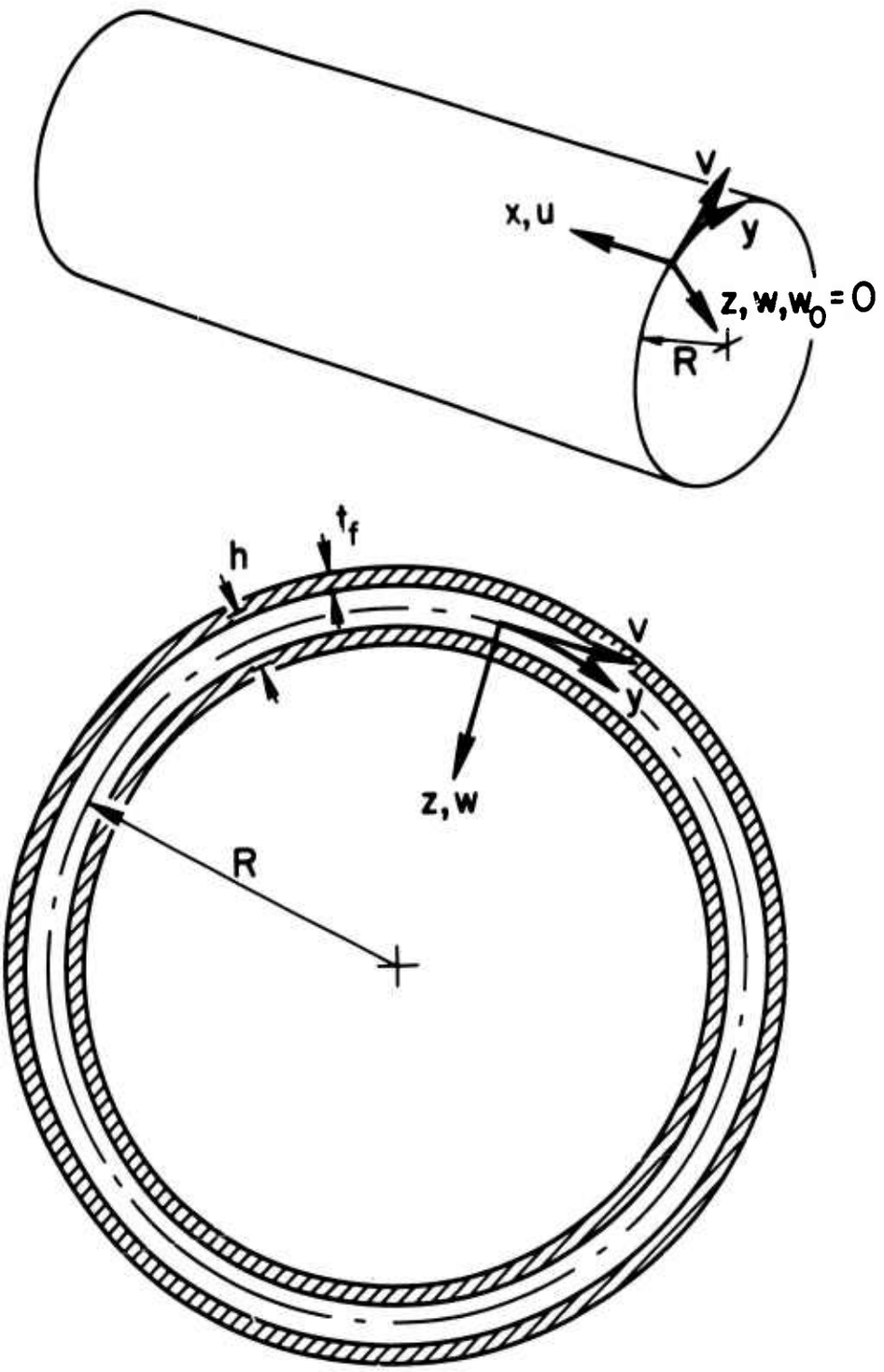

Figure 1. Circular Cylindrical Shell With Two-Element Cross Section.

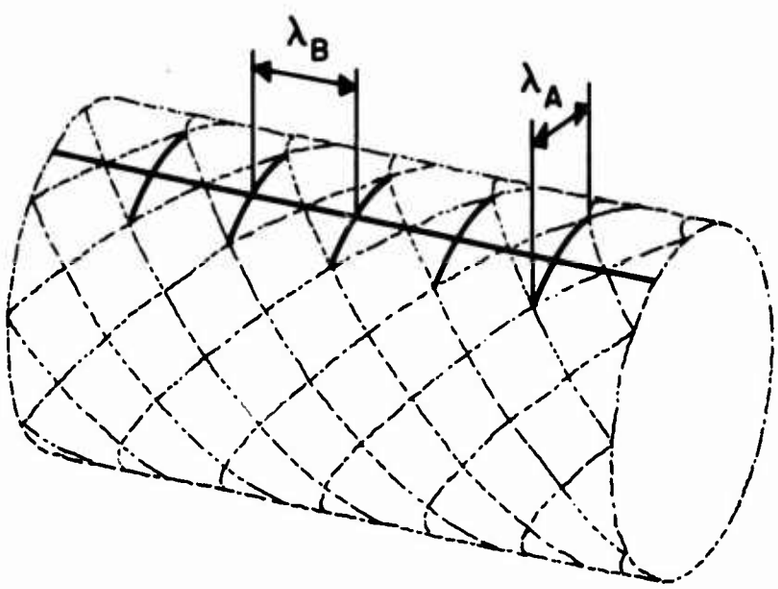

Figure 2. Beam-Arch Analog for Circular Cylindrical Shell. (Pure Diamond Nodal Pattern Shown for Illustrative Purposes Only. Shell Analysis Is Based on Ovalized Deflection Pattern.)

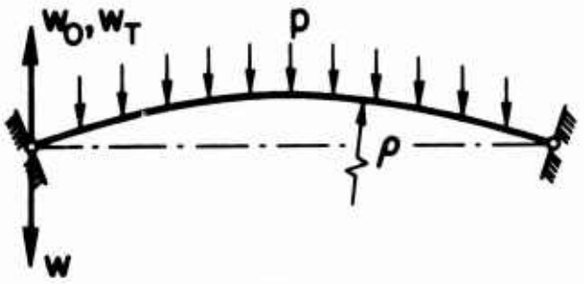

$$w_T = a_T \sin \frac{\pi y}{\lambda_A}$$

$$w_0 = a_0 \sin \frac{\pi y}{\lambda_A}$$

$$w = a \sin \frac{\pi y}{\lambda_A} = (a_T - a_0) \sin \frac{\pi y}{\lambda_A}$$

$$\bar{p} = \frac{ph}{EA}\left(\frac{R}{h}\right)^2$$

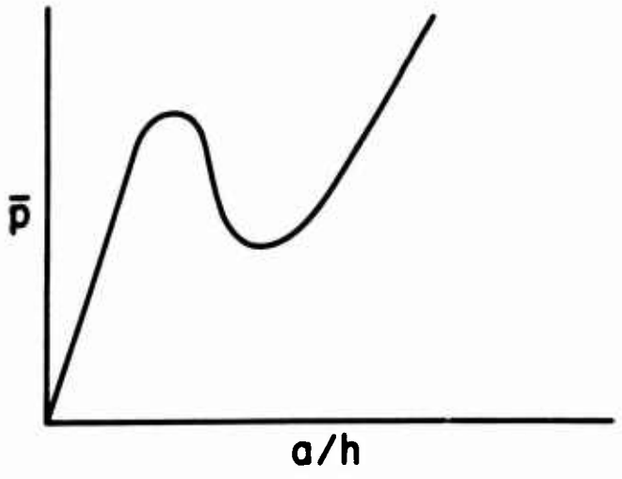

Figure 3. Load Deflection Relationship for Snap-Through Buckling of Shallow Arch.

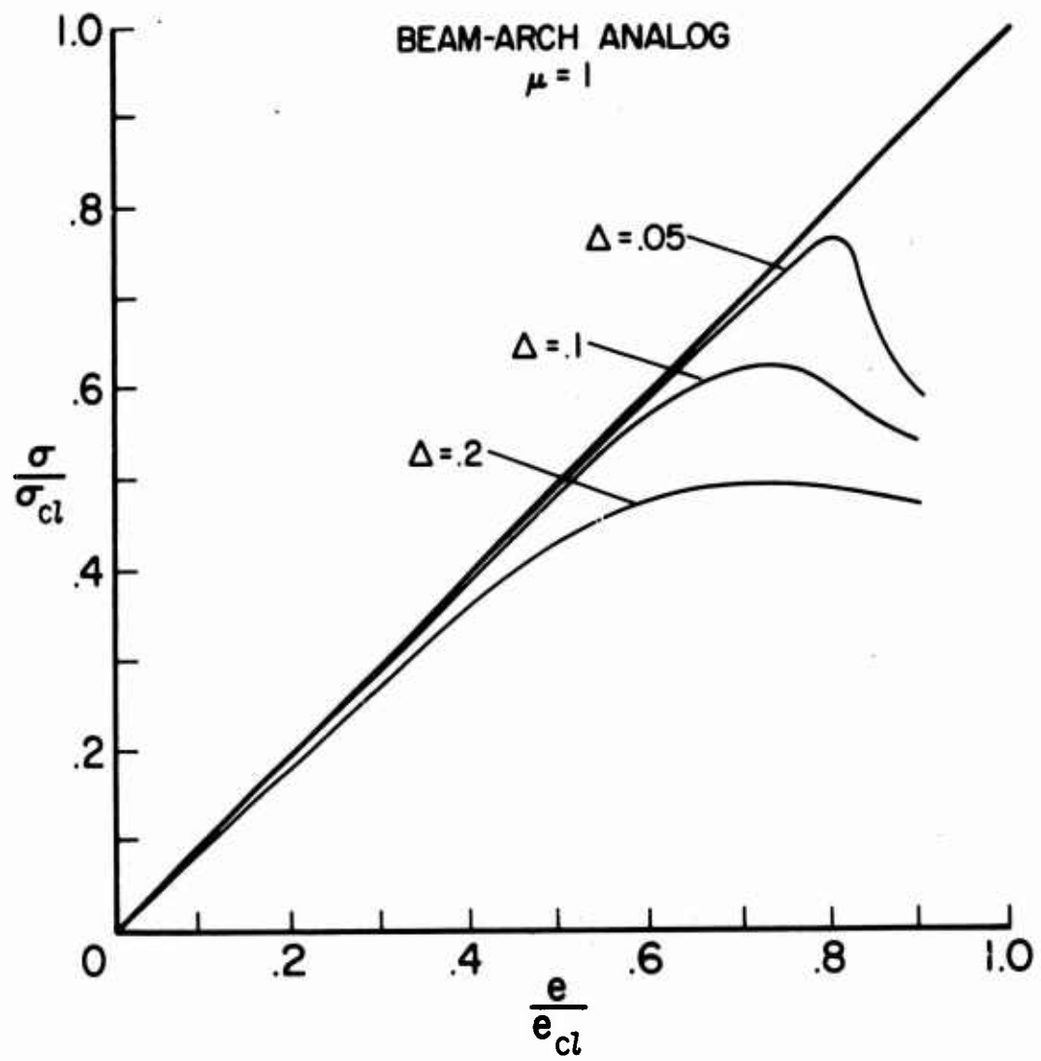

Figure 4. Load-Shortening Curves for the Beam-Arch Analog Obtained for Elastic Behavior.

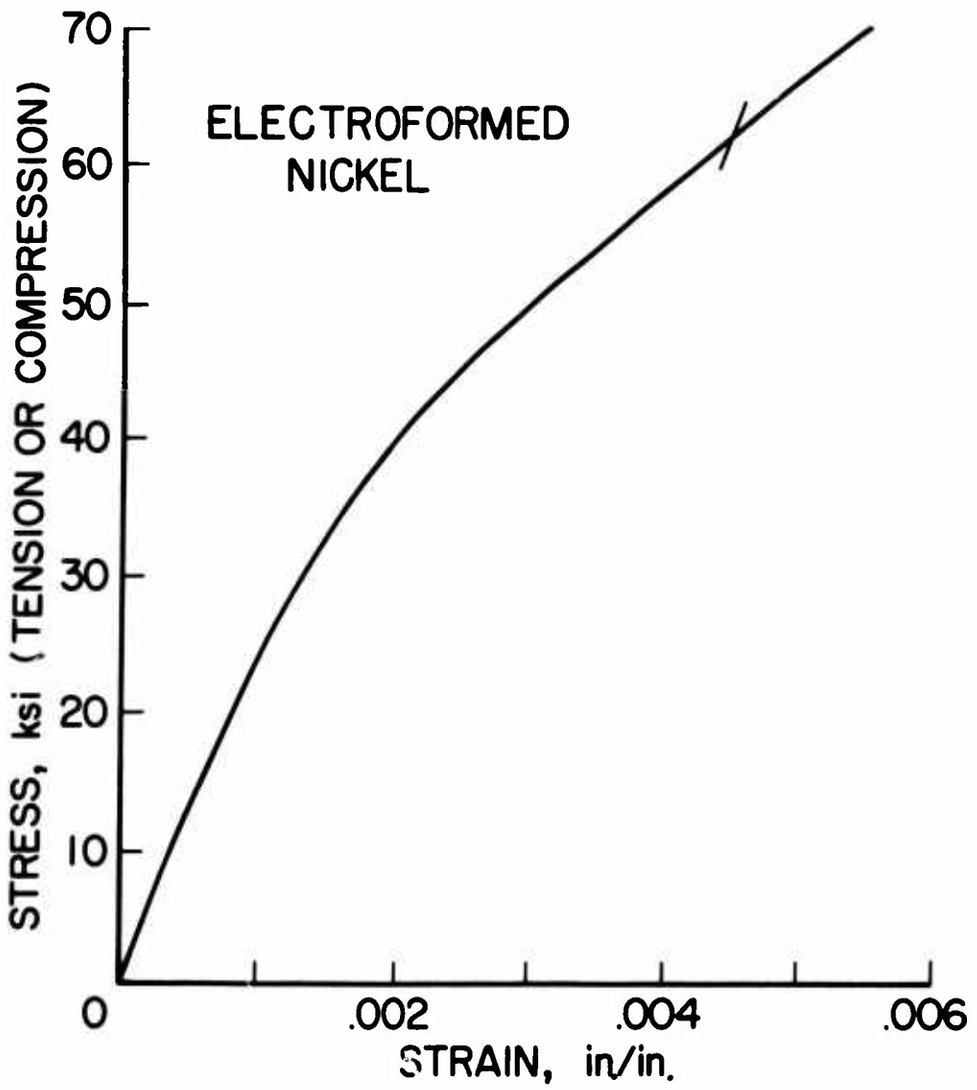

Figure 5. Stress-Strain Curve for Electroformed Nickel Utilized in Present Inelastic Analyses.

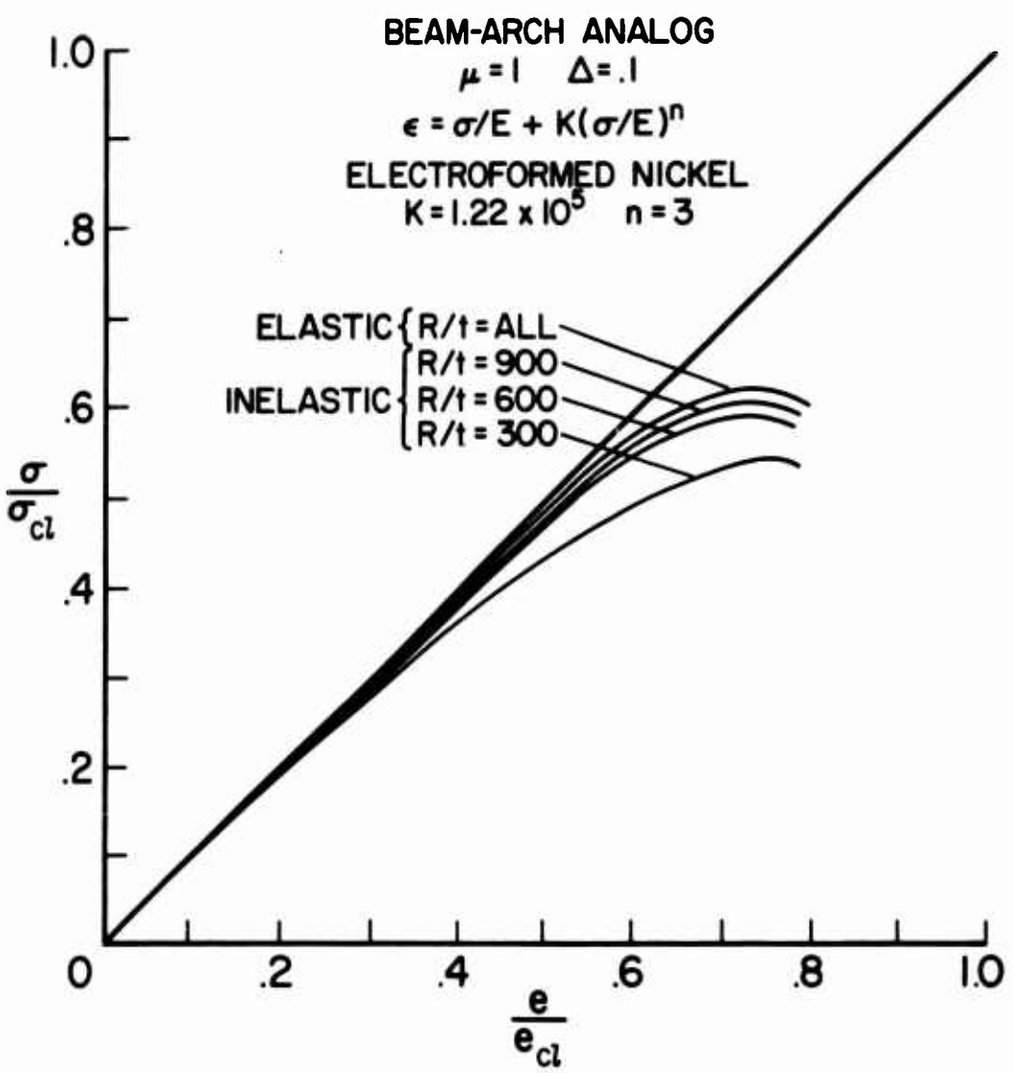

Figure 6. Family of Radius-to-Thickness-Dependent Load-Shortening Curves Corresponding to a Particular Imperfection Parameter for Electroformed Nickel Beam-Arch Analogs.

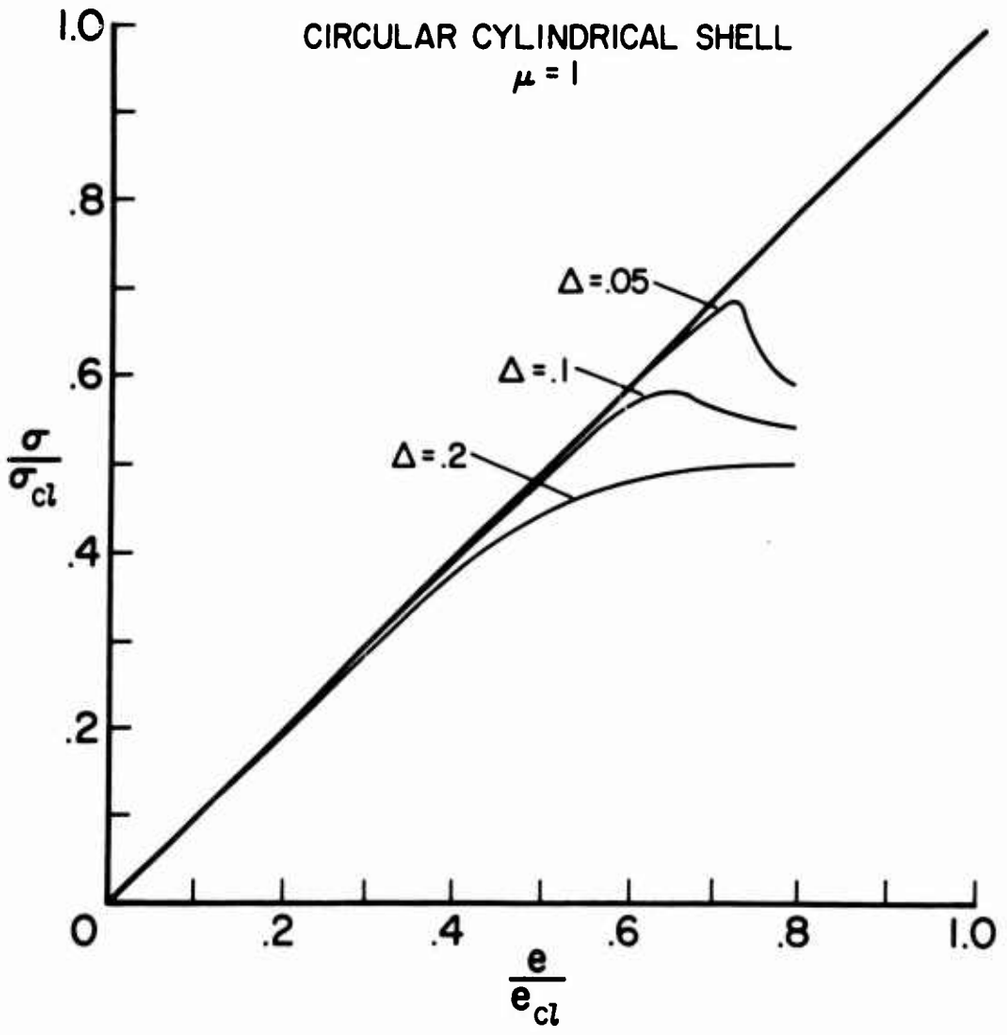

Figure 7. Load-Shortening Curves for a Circular Cylindrical Shell Obtained for Elastic Behavior.

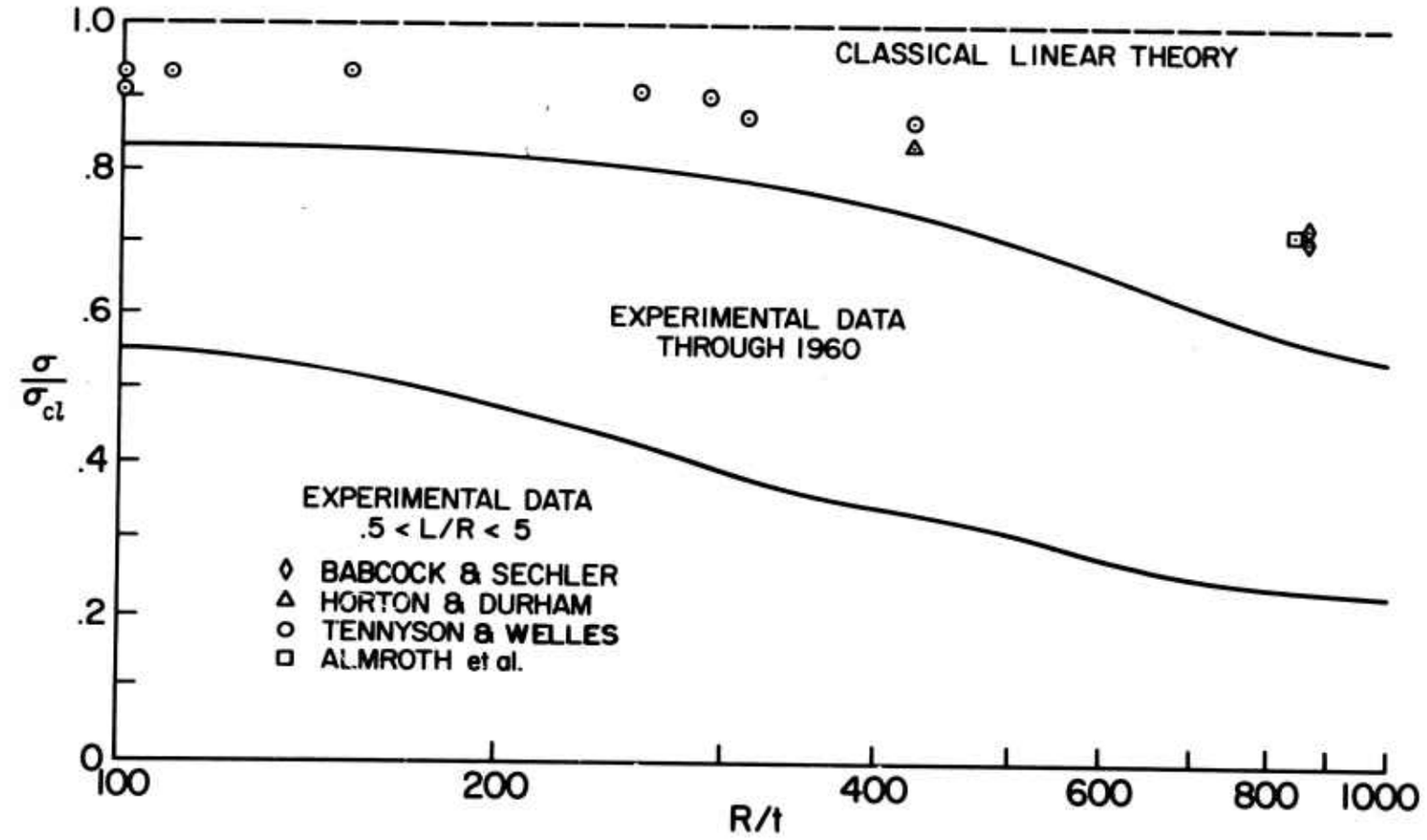

Figure 8. Experimental Buckling Loads for Axially Compressed, Circular Cylindrical Shells.

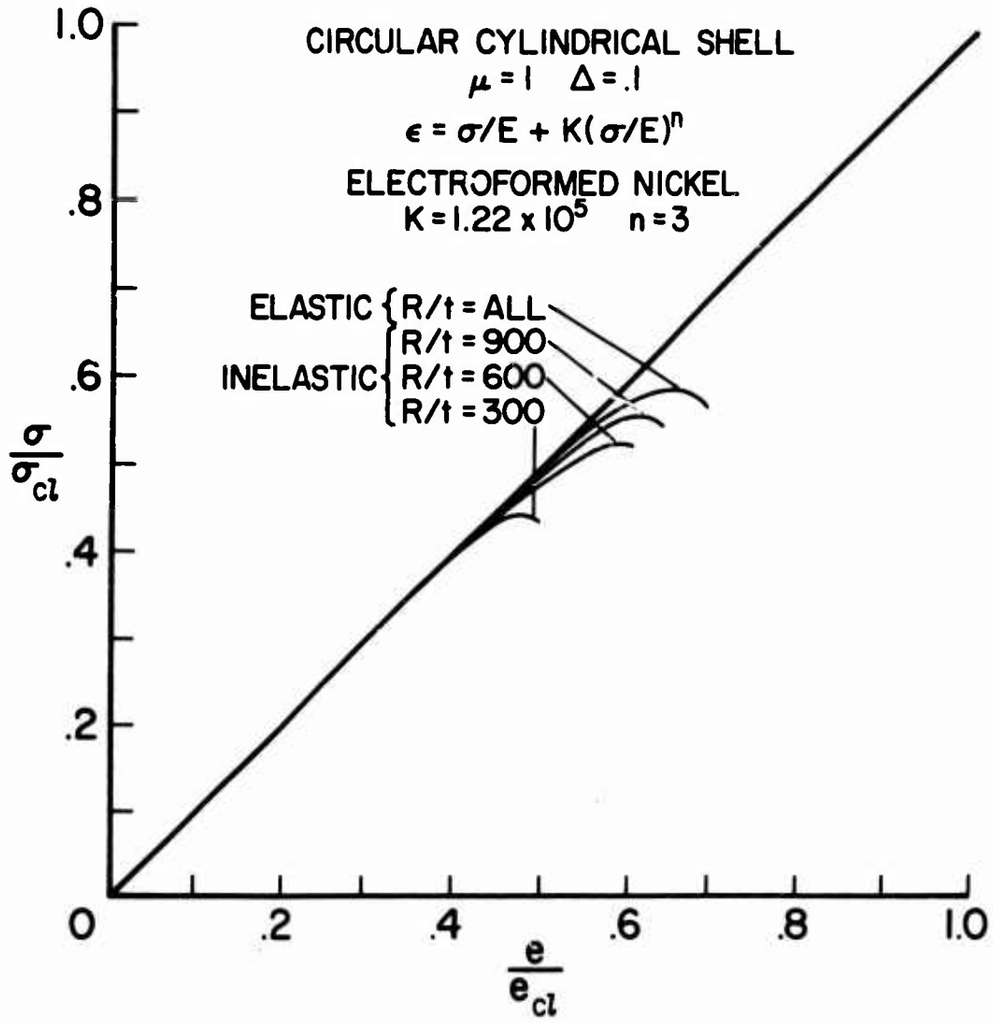

Figure 9. Family of Load-Shortening Curves for Electroformed Nickel Circular Cylindrical Shells.

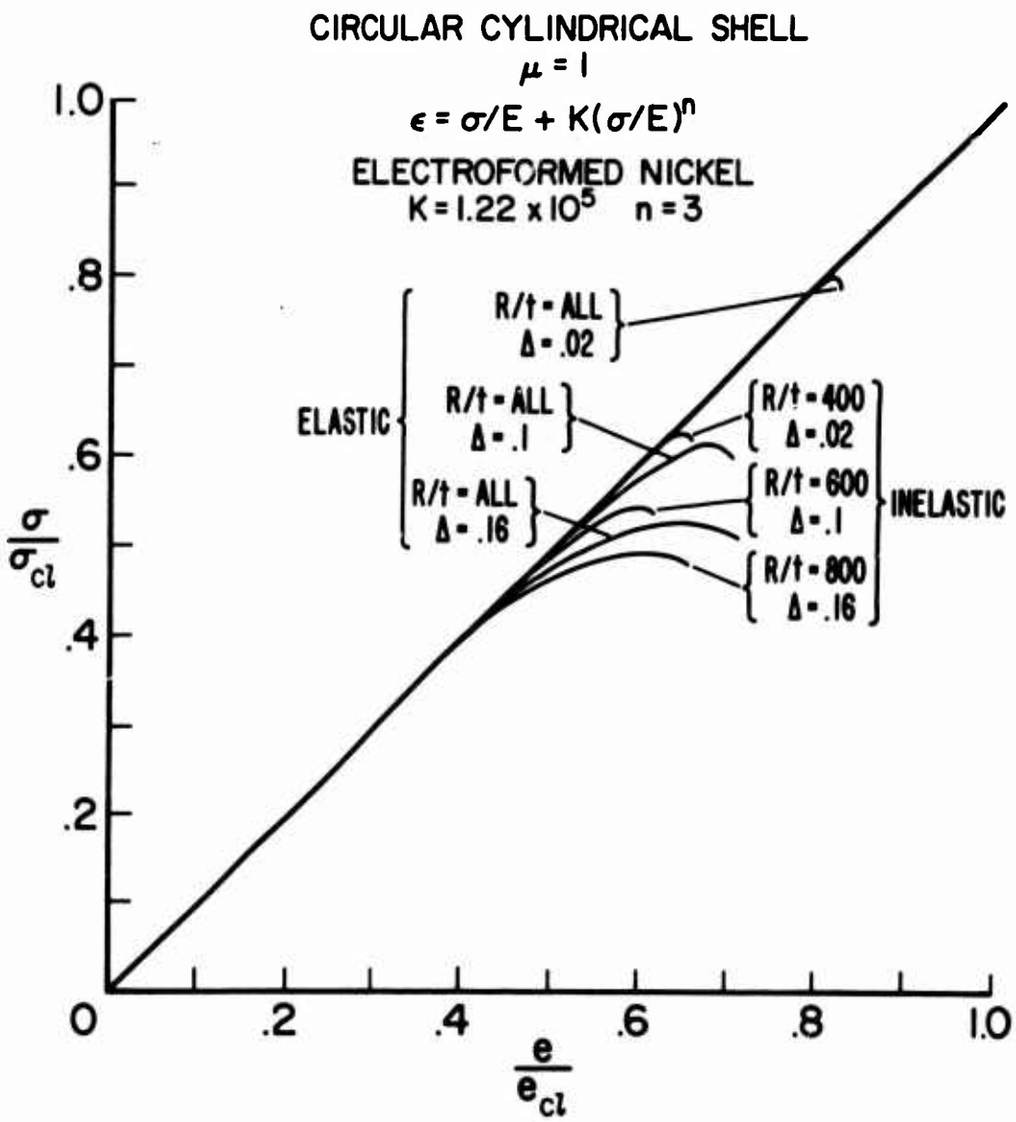

Figure 10. Families of Radius-to-Thickness-Dependent, Load-Shortening Curves Corresponding to Different Imperfection Parameters for Electroformed Nickel Circular Cylindrical Shells

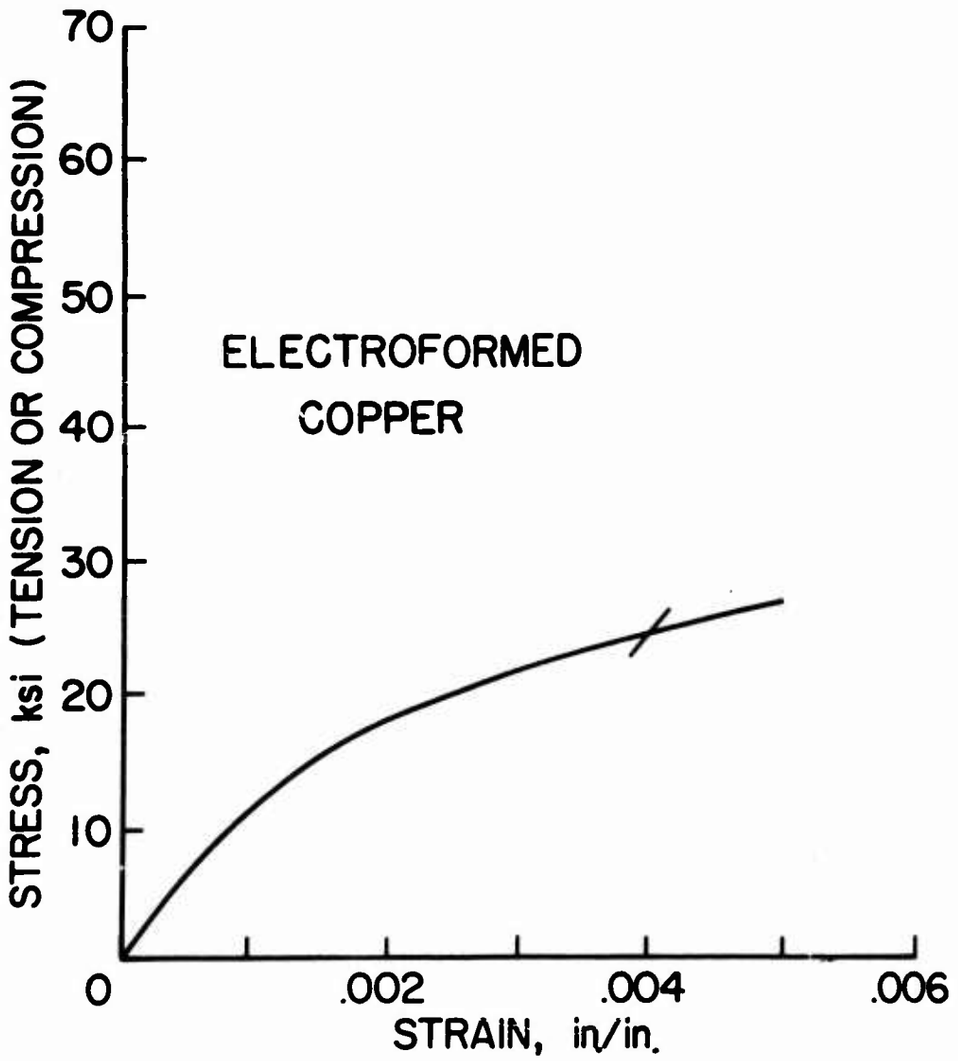

Figure 11. Stress-Strain Curve for Electroformed Copper Utilized in Present Inelastic Analyses.

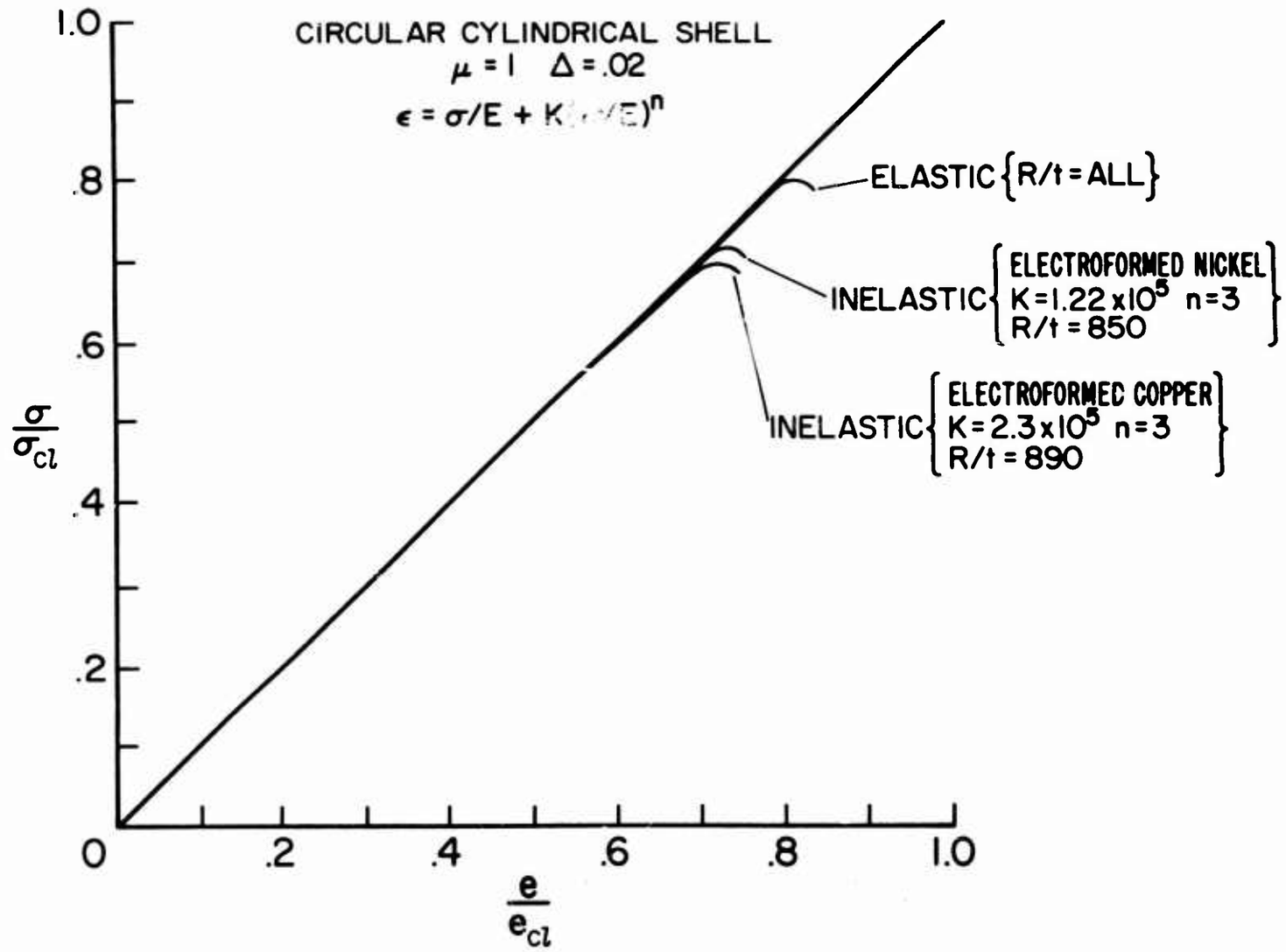

Figure 12. Family of Load-Shortening Curves for Electroformed Copper and Nickel Circular Cylindrical Shells.

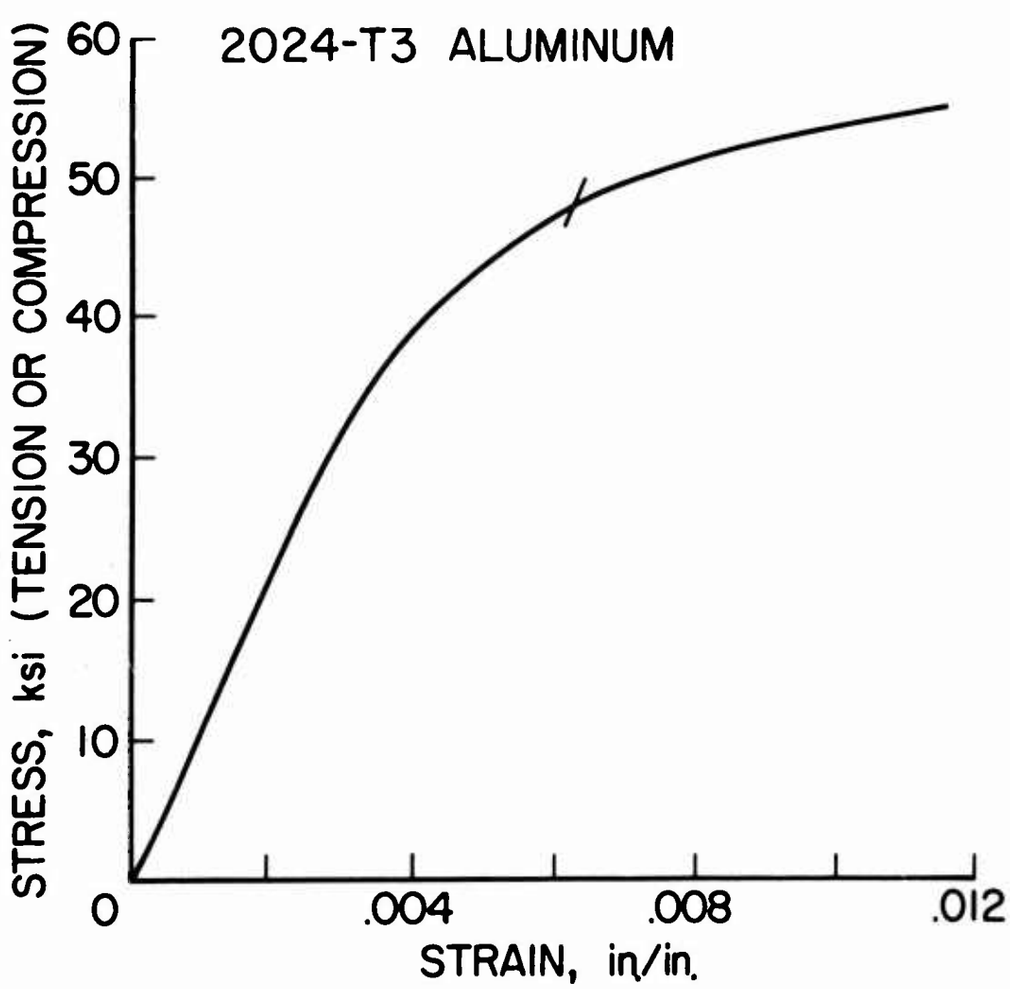

Figure 13. Stress-Strain Curve for Aluminum 2024-T3 Utilized in Present Inelastic Analyses.

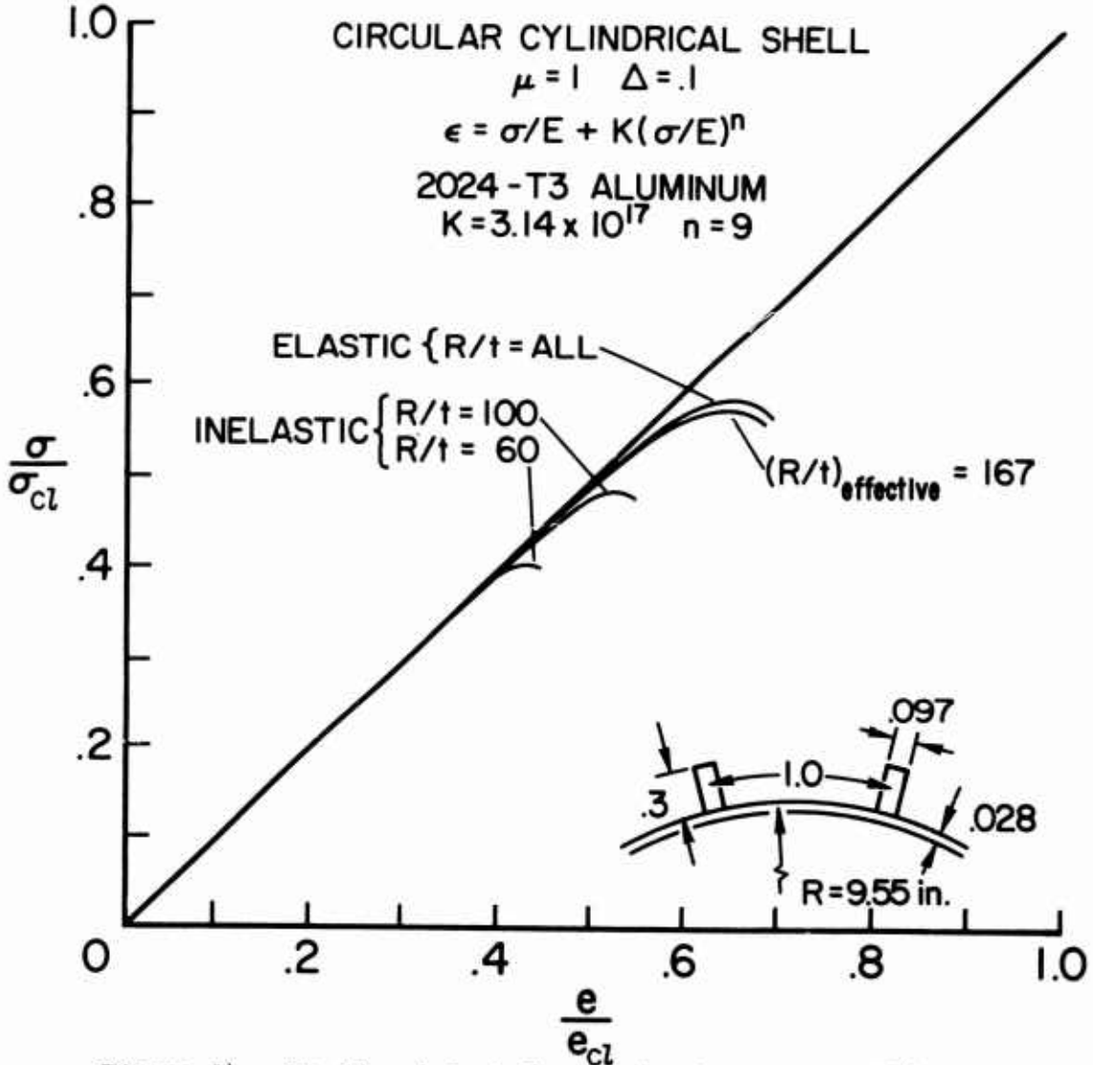

Figure 14. Family of Load-Shortening Curves for 2024-T3 Aluminum Circular Cylindrical Shells.

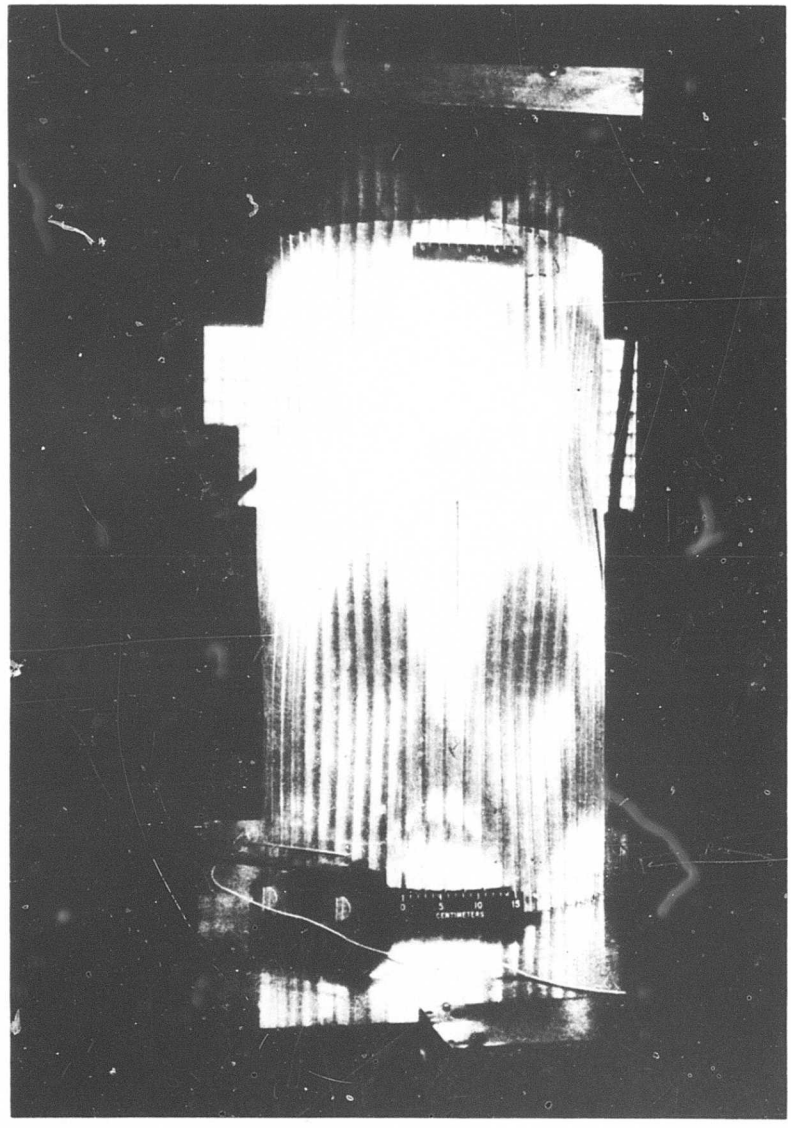

Figure 15. Buckled Stringer Stiffened, Circular Cylindrical Shell.

LITERATURE CITED

1. Hoff, N. J., THIN SHELLS IN AEROSPACE STRUCTURES, Fourth von Kármán Lecture Presented at the Third AIAA Annual Meeting, Nov. 29, 1966. Aeronautics and Astronautics, Feb. 1967, pp. 26-45.

2. Hoff, N. J., THE PERPLEXING BEHAVIOR OF THIN CIRCULAR CYLINDRICAL SHELLS IN AXIAL COMPRESSION, Second Theodore von Kármán Memorial Lecture of the Israel Society of Aeronautical Sciences, 1966.

3. Stein, M., RECENT ADVANCES IN THE INVESTIGATION OF SHELL BUCKLING, AIAA Journal, Vol. 6, No. 12, December 1968, pp. 2339-2345.

4. Donnell, L. H., A NEW THEORY FOR THE BUCKLING OF THIN CYLINDERS UNDER AXIAL COMPRESSION AND BENDING, Transactions of the American Society of Mechanical Engineers, Vol. 56, No. 11, November 1934, pp. 795-806.

5. Horton, W. H., and Durham, S. C., IMPERFECTIONS, A MAIN CONTRIBUTOR TO SCATTER IN EXPERIMENTAL VALUES OF BUCKLING LOAD, Int. J. Solids Structures, Vol. 1, 1965, pp. 59-72.

6. Weingarten, V. I., Morgan, E. J., and Seide, P., ELASTIC STABILITY OF THIN-WALLED CYLINDRICAL AND CONICAL SHELLS UNDER AXIAL COMPRESSION, AIAA Journal, Vol. 3, March 1965, pp 500-505.

7. Edwards, A. M., THE EFFECTS OF PLASTICITY ON THE BUCKLING AND POST-BUCKLING OF CIRCULAR CYLINDRICAL SHELLS; Thesis submitted for the degree of Doctor of Philosophy in Aeronautics and Astronautics to Stanford University, 1965.

8. Mayers, J., FAILURE CIRTERIONS FOR UNIFORMLY COMPRESSED THIN CYLINDRICAL AND SPHERICAL SHELLS POSTBUCKLING AGAINST RIGID MANDRELS, June 1964. (Unpublished).

9. Mayers, J., and Rehfield, L. W., DEVELOPMENTS IN MECHANICS, Vol. 3, Part 1, (Proceedings of the Ninth Midwestern Mechanics Conference, Madison, Wisconsin, August 16-18, 1965), New York, John Wiley and Sons, Inc., 1967, pp. 145-160.

10. Lee, L. H. N., INELASTIC BUCKLING OF INITIALLY IMPERFECT CYLINDRICAL SHELLS SUBJECT TO AXIAL COMPRESSION, Journal of Aerospace Sciences, January 1962, pp. 87-95.

11. Mayers, J., and Budiansky, B., ANALYSIS OF BEHAVIOR OF SIMPLY SUPPORTED FLAT PLATES COMPRESSED BEYOND BUCKLING INTO THE PLASTIC RANGE, National Advisory Committee for Aeronautics, NACA Technical Note No. 3368, 1955.

12. Mayers, J., Nelson, E., and Smith, L. B., MAXIMUM STRENGTH ANALYSIS OF POSTBUCKLED RECTANGULAR PLATES, Stanford University, Department of Aeronautics and Astronautics Report, SUDAAR No. 215, December 1964.

13. Mayers, J., and Nelson, E., MAXIMUM STRENGTH ANALYSIS OF POSTBUCKLED RECTANGULAR PLATES, Presented at AIAA Sixth Aerospace Sciences Meeting, AIAA Paper No. 68-171, New York, January 1968.

14. Reissner, E., ON A VARIATIONAL THEOREM IN ELASTICITY, Journal of Mathematics and Physics, Vol. 24, No. 2, July 1950, pp. 90-95.

15. Kempner, J., POSTBUCKLING BEHAVIOR OF AXIALLY COMPRESSED CIRCULAR CYLINDRICAL SHELLS, Journal of Aeronautical Sciences, Vol. 17, May 1954, pp. 329-335, 342.

16. Ramberg, W., and Osgood, W. R., DESCRIPTION OF STRESS-STRAIN CURVES BY THREE PARAMETERS, National Advisory Committee for Aeronautics, NACA Technical Note No. 902, 1943.

17. Cox, H. L., STRESS ANALYSIS OF THIN METAL CONSTRUCTION, The Journal of the Royal Aeronautical Society, Vol. 44, 1940, p. 231.

18. Tsien, H., BUCKLING OF A COLUMN WITH NONLINEAR LATERAL SUPPORTS, Journal of Aeronautical Sciences, Vol. 9, August 1942, pp. 373-384.

19. Hoff, N. J., A NONLINEAR MODEL STUDY OF THE THERMAL BUCKLING OF THIN ELASTIC SHELLS, Journal of Applied Mechanics, Vol. 32, March 1965, pp. 71-75.

20. Timoshenko, S., and Gere, J. M., THEORY OF ELASTIC STABILITY, 2nd Edition, New York, McGraw-Hill Co., 1961, p. 305.

21. Tennyson, R. C., and Welles, S. W., ANALYSIS OF THE BUCKLING PROCESS OF CIRCULAR CYLINDRICAL SHELLS UNDER AXIAL COMPRESSION, Institute of Aerospace Studies, University of Toronto, February 1968. (In process of publication in AIAA Journal).

22. Mayers, J., and Wrenn, B. G., DEVELOPMENTS IN MECHANICS, Vol. 4, (Proceedings of the Tenth Midwestern Mechanics Conference, Fort Collins, Colorado, August 21-23, 1967), Johnson Publishing Co., 1968, pp. 819-846.

23. Babcock, C. D., and Sechler, E. E., THE EFFECT OF INITIAL IMPERFECTIONS ON THE BUCKLING STRESS OF CIRCULAR CYLINDRICAL SHELLS, National Aeronautics and Space Administration, NASA Technical Note D-2005, July 1963.

24. Almroth, B.O., Holmes, A. M. C., and Brush, D. O., AN EXPERIMENTAL STUDY OF THE BUCKLING OF CYLINDERS UNDER AXIAL COMPRESSION, Experimental Mechanics, Vol. 4, September 1964, pp. 263-270.

25. Kanemitsu, S., and Nojima, N. M., AXIAL COMPRESSION TEST OF THIN-WALLED CIRCULAR CYLINDERS, Thesis submitted for the degree of Master of Science in Aeronautical Engineering to the California Institute of Technology, 1939.

26. Peterson, J. P., and Anderson, J. K., STRUCTURAL BEHAVIOR AND BUCKLING STRENGTH OF HONEYCOMB SANDWICH CYLINDERS SUBJECTED TO BENDING, National Aeronautics and Space Administration, NASA Technical Note D-2926, August 1965.

27. Cunningham, J. H., and Jacobson, M. J., DESIGN AND TESTING OF HONEYCOMB SANDWICH CYLINDERS UNDER AXIAL COMPRESSION, Collected Papers on Instability of Shell Structures - 1962, National Aeronautics and Space Administration, NASA Technical Note D-1510, December 1962, pp. 341-359.

28. Card, M. F., and Jones, R. M., EXPERIMENTAL AND THEORETICAL RESULTS FOR BUCKLING OF ECCENTRICALLY STIFFENED CYLINDERS, National Aeronautics and Space Administration, NASA Technical Note D-3639, October 1966.

29. Yoshimura, Y., ON THE MECHANISM OF BUCKLING OF A CIRCULAR CYLINDRICAL SHELL UNDER AXIAL COMPRESSION, National Advisory Committee for Aeronautics, NACA Technical Memorandum No. 1390, Washington, D. C., July 1955.

APPENDIX I

EULER EQUATIONS AND BOUNDARY CONDITIONS DERIVED FROM THE REISSNER FUNCTIONAL FOR A CYLINDER WITH PRESCRIBED END SHORTENING

The Reissner functional in the absence of prescribed surface loading is defined as

$$U'' = \iiint_V (\sigma_x \epsilon_x + \sigma_y \epsilon_y + \tau_{xy}\gamma_{xy} - F')dV \tag{40}$$

The strain-displacement relations of von Kármán-Donnell theory, modified for the two-element cylinder of Figure 1 and including initial radial deformation effects are

$$\epsilon_{x_{t,b}} = \epsilon'_x \pm \epsilon''_x = u_{,x} + \frac{1}{2} w_{,x}^2 + w_{o,x} w_{,x} \pm \frac{h}{2} w_{,xx}$$

$$\epsilon_{y_{t,b}} = \epsilon'_y \pm \epsilon''_y = v_{,y} - \frac{w}{R} + \frac{1}{2} w_{,y}^2 + w_{o,y} w_{,y} \pm \frac{h}{2} w_{,yy}$$

$$\gamma_{xy_{t,b}} = \gamma'_{xy} \pm \gamma''_{xy} = u_{,y} + v_{,x} + w_{,x} w_{,y} + w_{o,x} w_{,y} + w_{o,y} w_{,x}$$

$$\pm h w_{,xy} \tag{41}$$

The stresses in terms of midsurface and bending components are

$$\sigma_{x_{t,b}} = \sigma'_x \pm \sigma''_x$$

$$\sigma_{y_{t,b}} = \sigma'_y \pm \sigma''_y$$

$$\tau_{xy_{t,b}} = \tau'_{xy} \pm \tau''_{xy} \tag{42}$$

For the two-element section, equation (40) becomes

$$U'' = t_f \int_0^L \int_0^{2\pi R} \left\{ \sigma_{x_t} \epsilon_{x_t} + \sigma_{x_b} \epsilon_{x_b} + \sigma_{y_t} \epsilon_{y_t} + \sigma_{y_b} \epsilon_{y_b} + \tau_{xy_t} \gamma_{xy_t} + \tau_{xy_b} \gamma_{xy_b} - (F_t' + F_b') \right\} dxdy \tag{43}$$

Then, in view of equations (41) and (42), equation (43) may be written as

$$\begin{aligned} U'' = t_f \int_0^L \int_0^{2\pi R} \Big\{ & \left(\sigma_{x_t} + \sigma_{x_b}\right) \left[u_{,x} + \tfrac{1}{2} w_{,x}^2 + w_{o,x} w_{,x} \right] \\ & + \left(\sigma_{y_t} + \sigma_{y_b}\right) \left[v_{,y} + \tfrac{1}{2} w_{,y}^2 + w_{o,y} w_{,y} - \frac{w}{R} \right] \\ & + \left(\tau_{xy_t} + \tau_{xy_b}\right) \Big[u_{,y} + v_{,x} + w_{,x} w_{,y} \\ & + w_{o,x} w_{,y} + w_{o,y} w_{,x} \Big] + \left(\sigma_{x_t} - \sigma_{x_b}\right) \left[\tfrac{h}{2} w_{,xx} \right] \\ & + \left(\sigma_{y_t} - \sigma_{y_b}\right) \left[\tfrac{h}{2} w_{,yy} \right] + \left(\tau_{xy_t} - \tau_{xy_b}\right) \left[h w_{,xy} \right] - (F_t' + F_b') \Big\} dxdy \end{aligned} \tag{44}$$

The average stresses and the bending moments are

$$\sigma_x' = \tfrac{1}{2}(\sigma_{x_t} + \sigma_{x_b})$$

$$\sigma_y' = \tfrac{1}{2}(\sigma_{y_t} + \sigma_{y_b})$$

$$\tau_{xy}' = \tfrac{1}{2}(\tau_{xy_t} + \tau_{xy_b})$$

$$M_x = -t_f \tfrac{h}{2}(\sigma_{x_t} - \sigma_{x_b}) = -t_f h \sigma_x''$$

$$M_y = -t_f \tfrac{h}{2}(\sigma_{y_t} - \sigma_{y_b}) = -t_f h \sigma_y''$$

$$M_{xy} = t_f \tfrac{h}{2}(\tau_{xy_t} - \tau_{xy_b}) = t_f h \tau_{xy}'' \tag{45}$$

Substitution of equation (45) into equation (44) gives

$$U'' = 2t_f \int_0^L \int_0^{2\pi R} \Big\{ \sigma_x'(u_{,x} + \tfrac{1}{2} w_{,x}^2 + w_{o,x} w_{,x}) + \sigma_y'(v_{,y} + \tfrac{1}{2} w_{,y}^2 + w_{o,y} w_{,y} - \frac{w}{R}) + \tau_{xy}'(v_{,x} + u_{,y} + w_{,x} w_{,y} + w_{o,x} w_{,y} + w_{o,y} w_{,x}) - \frac{M_x}{2t_f} w_{,xx} - \frac{M_y}{2t_f} w_{,yy} + \frac{M_{xy}}{t_f} w_{,xy} - F' \Big\} \, dxdy \qquad (46)$$

With cognizance taken of the fact that

$$\delta F' = \frac{\partial F'}{\partial \sigma_x} \delta\sigma_x + \frac{\partial F'}{\partial \sigma_y} \delta\sigma_y + \frac{\partial F'}{\partial \tau_{xy}} \delta\tau_{xy}$$

or

$$\delta F' = \frac{\partial F'}{\partial \sigma_x'} \delta\sigma_x' + \frac{\partial F'}{\partial \sigma_y'} \delta\sigma_y' + \frac{\partial F'}{\partial \tau_{xy}'} \delta\tau_{xy} + \frac{\partial F'}{\partial M_x} \delta M_x + \frac{\partial F'}{\partial M_y} \delta M_y + \frac{\partial F'}{\partial M_{xy}} \delta M_{xy}$$

then the vanishing of the first variation of U'' with respect to σ_x', σ_y', τ_{xy}', M_x, M_y, M_{xy}, u, v, and w requires that

$$\delta U'' = 2t_f \int_0^L \int_0^{2\pi R} \Big\{ \delta\sigma_x'(u_{,x} + \tfrac{1}{2} w_{,x}^2 + w_{,x} w_{o,x}) + \delta\sigma_y'(v_{,y} + \tfrac{1}{2} w_{,y}^2 + w_{,y} w_{o,y} - \frac{w}{R}) + \delta\tau_{xy}'(v_{,x} + u_{,y} + w_{,x} w_{,y} + w_{o,x} w_{,y} + w_{o,y} w_{,x}) + \sigma_x'(\delta u_{,x} + w_{,x} \delta w_{,x} + w_{o,x} \delta w_{,x}) + \sigma_y'(\delta v_{,y} + w_{,y} \delta w_{,y} + w_{o,y} \delta w_{,y}) - \sigma_y' \frac{\delta w}{R} + \tau_{xy}'(\delta v_{,x} + \delta u_{,y} + \delta w_{,x} w_{,y} + w_{,x} \delta w_{,y}$$

$$
\begin{aligned}
&+ w_{o,x}\delta w_{,y} + w_{o,y}\delta w_{,x}) \\
&- \frac{\delta M_x}{2t_f} w_{,xx} - \frac{\delta M_y}{2t_f} w_{,yy} + \frac{\delta M_{xy}}{t_f} w_{,xy} \\
&- \frac{M_x}{2t_f} \delta w_{,xx} - \frac{M_y}{2t_f} \delta w_{,yy} + \frac{M_{xy}}{t_f} \delta w_{,xy} \\
&-\Big[\frac{\partial F'}{\partial \sigma'_x} \delta\sigma'_x + \frac{\partial F'}{\partial \sigma'_y} \delta\sigma'_y + \frac{\partial F'}{\partial \tau'_{xy}} \delta\tau'_{xy} \\
&+ \frac{\partial F'}{\partial M_x} \delta M_x + \frac{\partial F'}{\partial M_y} \delta M_y + \frac{\partial F'}{\partial M_{xy}} \delta M_{xy} \Big]\Big\} dxdy = 0
\end{aligned}
\tag{47}
$$

The result of carrying out the integration by parts is

$$
\begin{aligned}
\delta U'' = 2t_f \int_0^L \int_0^{2\pi R} \Big\{ & (u_{,x} + \tfrac{1}{2} w_{,x}^2 + w_{,x} w_{o,x} - \frac{\partial F'}{\partial \sigma'_x}) \delta\sigma'_x \\
& + (v_{,y} + \tfrac{1}{2} w_{,y}^2 + w_{,y} w_{o,y} - \frac{w}{R} - \frac{\partial F'}{\partial \sigma'_y}) \delta\sigma'_y \\
& + (v_{,x} + u_{,y} + w_{,x} w_{,y} + w_{o,x} w_{,y} + w_{o,y} w_{,x} \\
& - \frac{\partial F'}{\partial \tau'_{xy}}) \delta\tau'_{xy} - (\frac{1}{2t_f} w_{,xx} + \frac{\partial F'}{\partial M_x}) \delta M_x \\
& - (\frac{1}{2t_f} w_{,yy} + \frac{\partial F'}{\partial M_y}) \delta M_y \\
& - (\frac{1}{t_f} w_{,xy} + \frac{\partial F'}{\partial M_{xy}}) \delta M_{xy} - (\sigma'_{x,x} + \tau_{xy,y}) \delta u \\
& - (\sigma'_{y,y} + \tau'_{xy,x}) \delta v - [(\sigma'_x [w_{,x} + w_{o,x}])_{,x} \\
& + (\sigma'_y [w_{,y} + w_{o,y}])_{,y} + (\tau'_{xy} [w_{,y} + w_{o,y}])_{,x} \\
& + (\tau'_{xy} [w_{,x} + w_{o,x}])_{,y} + \frac{\sigma'_y}{R} \\
& + 2t_f (M_{x,xx} + M_{y,yy} - 2M_{xy,xy})] \delta w \Big\} dxdy \\
& + 2t_f \int_0^{2\pi R} \sigma'_x \delta u \Big|_0^L dy + 2t_f \int_0^L \sigma'_y \delta v \Big|_0^{2\pi R} dx
\end{aligned}
$$

$$+ 2t_f \int_0^{2\pi R} [\sigma'_x(w_{,x} + w_{o,x}) + \tau'_{xy}(w_{,y} + w_{o,y})$$

$$+ \frac{1}{2t_f} M_{x,x} - \frac{1}{t_f} M_{xy,y}]\delta w \Big|_0^L dy$$

$$+ 2t_f \int_0^{2\pi R} \tau'_{xy} \delta v \Big|_0^L dy + 2t_f \int_0^L \tau'_{xy} \delta u \Big|_0^{2\pi R} dx$$

$$+ 2t_f \int_0^L [\sigma'_y(w_{,y} + w_{o,y}) + \tau'_{xy}(w_{,x} + w_{o,x})$$

$$+ \frac{1}{2t_f} M_{y,y} - \frac{1}{t_f} M_{xy,x}]\delta w \Big|_0^{2\pi R} dx$$

$$- \int_0^{2\pi R} M_x \delta w_{,x} \Big|_0^L dy - \int_0^L M_y \delta w_{,y} \Big|_0^{2\pi R} dx$$

$$+ 2M_{xy} \delta w \Big|_{0\,0}^{L\;2\pi R} = 0 \qquad (48)$$

For equation (48) to vanish for arbitrary variations in the states of stress and displacement, consistent with prescribed displacement boundary conditions, each of the above terms must vanish identically. The Euler equations which result are

Stress-displacement relations:

$$\frac{\partial F'}{\partial \sigma'_x} = u_{,x} + \frac{1}{2} w_{,x}^2 + w_{o,x} w_{,x}$$

$$\frac{\partial F'}{\partial \sigma'_y} = v_{,y} + \frac{1}{2} w_{,y}^2 + w_{o,y} w_{,y} - \frac{w}{R}$$

$$\frac{\partial F'}{\partial \tau'_{xy}} = v_{,x} + u_{,y} + w_{,x} w_{,y} + w_{o,y} w_{,y} + w_{o,y} w_{,x} \qquad (49)$$

Moment-curvature relations:

$$\frac{\partial F'}{\partial M_x} = -\frac{1}{2t_f} w_{,xx}$$

$$\frac{\partial F'}{\partial M_y} = -\frac{1}{2t_f} w_{,yy}$$

$$\frac{\partial F'}{\partial M_{xy}} = -\frac{1}{t_f} w_{,xy} \tag{50}$$

Midsurface equilibrium equations:

$$\sigma'_{x,x} + \tau'_{xy,y} = 0$$

$$\sigma'_{y,y} + \tau'_{xy,x} = 0 \tag{51}$$

Lateral equilibrium equation:

$$(\sigma'_x[w_{,x} + w_{o,x}])_{,x} + (\sigma'_y[w_{,y} + w_{o,y}])_{,y}$$

$$+(\tau'_{xy}[w_{,y} + w_{o,y}])_{,x} + (\tau'_{xy}[w_{,x} + w_{o,x}])_{,y}$$

$$+ \frac{\sigma'_y}{R} + \frac{1}{2t_f}[M_{x,xx} + M_{y,yy} - 2M_{xy,xy}] = 0 \tag{52}$$

In view of equation (51), the lateral equilibrium equation (52) becomes

$$\sigma'_x(w_{,xx} + w_{o,xx}) + \sigma'_y(w_{,yy} + w_{o,yy})$$

$$+ 2\tau'_{xy}(w_{,xy} + w_{o,xy}) + \frac{\sigma'_y}{R}$$

$$+ \frac{1}{2t_f}(M_{x,xx} + M_{y,yy} - 2M_{xy,xy}) = 0 \tag{53}$$

which, for a homogeneous, isotropic body ($2t_f \to t$) and Hookean material, reduces to the well-known lateral equilibrium equation of von Kármán-Donnell theory (see, for example, ref. 15).

The midsurface stress-displacement boundary integrals are

$$\int_0^{2\pi R} \sigma_x' \delta u \Big|_0^L \, dy = 0 \tag{54a}$$

$$\int_0^{2\pi R} \tau_{xy}' \delta v \Big|_0^L \, dy = 0 \tag{54b}$$

$$\int_0^{L} \sigma_y' \delta v \Big|_0^{2\pi R} \, dx = 0 \tag{54c}$$

$$\int_0^{L} \tau_{xy}' \delta u \Big|_0^{2\pi R} \, dx = 0 \tag{54d}$$

The remaining boundary integrals are

$$2t_f \int_0^{2\pi R} \left\{ \sigma_x' (w_{,x} + w_{o,x}) + \tau_{xy}' (w_{,y} + w_{o,y}) + \frac{1}{2t_f} M_{x,x} - \frac{1}{t_f} M_{xy,y} \right\} \delta w \Big|_0^L \, dy = 0 \tag{55a}$$

$$2t_f \int_0^{L} \left\{ \sigma_y' (w_{,y} + w_{o,y}) + \tau_{xy}' (w_{,x} + w_{o,x}) + \frac{1}{2t_f} M_{y,y} - \frac{1}{t_f} M_{xy,x} \right\} \delta w \Big|_0^{2\pi R} \, dx = 0 \tag{55b}$$

$$2M_{xy} \delta w \Big|_0^L \Big|_0^{2\pi R} = 0 \tag{55c}$$

For the present problem, that of a long, circular cylindrical shell, the end shortening is prescribed; thus δu vanishes at $x = 0, L$. The remaining boundary conditions at $x = 0, L$ can be ignored due to the length assumed for the shell. The boundary conditions at $y = 0, 2\pi R$ are either continuity conditions (55a, b, and c) or conditions which preclude the transfer of any circumferential and shear loads across a generator (54 c, d).

APPENDIX II

SHALLOW-ARCH AND BEAM-ARCH LOAD-SHORTENING RELATIONSHIPS

SHALLOW ARCH

The expressions for the displacements and stresses [equation (20)] can be substituted into the Reissner functional given by equation (19). Upon subsequent integration, the Reissner functional for a shallow arch under uniform loading is then

$$\bar{U}''_A = \frac{U''_A + V''_A}{VE(h/r)^2} = -\frac{\sigma_A R}{Eh}\frac{\eta}{16}\left(\xi^2 - \frac{\pi^2}{\eta}\xi\right) - \frac{\sigma_{1A}}{48E}(R/h)\eta\xi - \frac{1}{12}\left(\frac{\sigma_A R}{Eh}\right)^2 - \frac{1}{12}\left(\frac{\sigma_{1A}}{E}\frac{R}{h}\right)^2 - \frac{2}{\pi}\bar{p}\xi \tag{56}$$

where

$$\xi = a/h$$

$$\eta = \frac{4\pi^2 Rh}{\lambda_A^2} = \frac{\pi^2}{2}\left(\frac{h}{a_o}\right)$$

$$\bar{p} = \frac{ph}{EA}\left(\frac{R}{h}\right)^2$$

The first variation of $\bar{U}''_A$ with respect to σ_A, σ_{1A}, and ξ results in

$$\frac{\sigma_A R}{Eh} = -\frac{\eta}{16}\left(\xi^2 - \frac{\pi^2}{\eta}\xi\right) \tag{57}$$

$$\frac{\sigma_{1A} R}{Eh} = -\frac{\eta}{8}\xi \tag{58}$$

and

$$-\frac{\sigma_A R}{Eh}\frac{\eta}{16}\left(2\xi - \frac{\pi^2}{\eta}\right) - \frac{\sigma_{1A} R}{Eh}\frac{\eta}{48} - \frac{2}{\pi}\bar{p} = 0 \tag{59}$$

These simultaneous equations can be written in terms of ξ alone as

$$\xi^3 - \frac{3\pi^2}{2\eta}\xi^2 + \left(\frac{\pi^4}{2\eta^2} + \frac{1}{3}\right)\xi = \left(\frac{16}{\eta}\right)^2\frac{\bar{p}}{\pi} \tag{60}$$

For prescribed values of η and $\bar{p}$, equation (60) can be solved numerically for ξ. The results are shown in a plot of $\bar{p}$ vs. ξ in the lower portion of Figure 3.

BEAM-ARCH ANALOG

The expressions for the displacements and stresses [equations (20) and (23)] can be substituted into the Reissner functional given by equation (22). The result of integrating the Reissner functional for a two-element beam arch is

$$\bar{U}'' = \frac{U_B'' + U_A''}{VE(h/R)^2} = -\frac{\sigma R}{Eh}\left(-\frac{eR}{h} + \frac{\xi^2\mu^2\eta}{16} + \frac{\xi\delta_o\mu^2\eta}{8}\right)$$
$$-\frac{\sigma_1 R}{Eh}\frac{\xi\mu^2\eta}{16} - \frac{1}{2}\left(\frac{\sigma R}{Eh}\right)^2 - \frac{1}{4}\left(\frac{\sigma_1 R}{Eh}\right)^2 - \left(\frac{\sigma_A R}{Eh}\right)\frac{\eta}{16}\left(\xi^2 - \frac{\pi^2}{\eta}\xi\right)$$
$$-\frac{\sigma_{1A}\eta\xi}{E16}\frac{R}{h} - \frac{1}{2}\left(\frac{\sigma_A R}{Eh}\right)^2 - \frac{1}{4}\left(\frac{\sigma_{1A} R}{Eh}\right)^2 \qquad (61)$$

where

ξ = a/h

δ_o = a_o/h

μ = λ_A/λ_B

e = applied unit end shortening

The first variation of $\bar{U}''$ with respect to σ, σ_1, ξ, σ_A, and σ_{1A} results in

$$\frac{\sigma R}{Eh} = \frac{eR}{h} - \frac{\mu^2\eta}{16}(\xi^2 + 2\xi\delta_o) \qquad (62)$$

$$\frac{\sigma_1 R}{Eh} = -\frac{\mu^2\eta}{8}\xi \qquad (63)$$

$$\frac{\sigma_A R}{Eh} = -\frac{\eta}{16}\left(\xi^2 - \frac{\pi^2}{\eta}\xi\right) \qquad (64)$$

$$\frac{\sigma_{1A} R}{Eh} = -\frac{\eta}{8}\xi \qquad (65)$$

$$-\frac{\sigma R}{Eh}\frac{\mu^2\eta}{8}(\xi + \delta_o) \quad -\frac{\sigma_1 R}{Eh}\frac{\mu^2\eta}{16}$$

(continued)

$$- \frac{\sigma_A R}{Eh}\left(\frac{\eta}{16}\right)\left(2\xi - \frac{\pi^2}{\eta}\right) - \frac{\sigma_{1A} R}{Eh}\frac{\eta}{16} = 0 \qquad (66)$$

The above equations can be written in terms of the parameter ξ alone as

$$\xi^3\left[1 + \frac{1}{\mu^4}\right] + \xi^2\left[3\delta_o - \frac{3\pi^2}{2\eta\mu^4}\right]$$

$$+ \xi\left[-\frac{16}{\mu^2\eta}\frac{eR}{h} + 2\left(\delta_o^2 + \frac{\pi^4}{4\eta^2\mu^4}\right) + 1 + \frac{1}{\mu^4}\right]$$

$$- 16\frac{\delta_o}{\mu^2\eta}\frac{eR}{h} = 0 \qquad (67)$$

For prescribed values of μ, η, δ_o, and eR/h, equation (67) can be solved numerically for ξ. Then, for the same parameter values and corresponding ξ's, equation (62) can be solved numerically to establish the load-shortening relationship between $\sigma R/Eh$ and eR/h and to develop the curves shown in Figure 4.

APPENDIX III

METHOD OF SOLUTION FOR ELASTIC CIRCULAR CYLINDRICAL SHELL

After the expressions for the assumed displacements [equations (26), (27), and (28)] and stresses [equations (29), (30), and (31)] are substituted into the Reissner functional given by equation (18), subsequent integration yields

$$\begin{aligned}\overline{U}'' = \frac{U''}{Et(\frac{2\pi RL}{4})} = &-4\frac{\sigma}{E}F_{0C} - A_{02}F_{02} - A_{11}(F_{11}+H_{11}) \\ &-4A_{22}(F_{22}+H_{22}) - 3A_{31}(F_{31}+3H_{31}) \\ &-A_{13}(3F_{13}+H_{13}) - 8A_{20}H_{20} \\ &-2\left(\frac{\sigma}{E}\right)^2 - \frac{1}{2}[(A_{11}^2+16A_{22}^2)(1+\mu^2)^2 + A_{13}^2(9+\mu^2)^2 \\ &+ A_{31}^2(1+9\mu^2)^2 + 32(A_{02}^2+\mu^4A_{20}^2)] \\ &+ \frac{\eta^2(t/R)^2}{24(1-\nu^2)}[(1+\mu^2)^2\xi_1^2 + 32(\mu^4\xi_2^2+\xi_3^2)] + 4\frac{\sigma}{E}e \end{aligned} \tag{68}$$

where the F's and H's are defined as

$$F_{00} = \mu^2\eta\frac{t}{R}[\frac{\xi_{11}^2}{8} + \xi_{20}^2 + 2\xi_{11_o}(\frac{\xi_{11}}{8}+\frac{\xi_{20}}{4})]$$

$$F_{02} = \mu^2\eta\frac{t}{R}[\xi_{11}^2 + 2\xi_{11_o}\xi_{11}]$$

$$F_{11} = \mu^2\eta\frac{t}{R}[2\xi_{11}\xi_{20}+\xi_{11}\xi_{02}+2\xi_{11_o}(\xi_{20}+\frac{\xi_{02}}{2} + \frac{\xi_{11}}{4})]$$

$$F_{22} = \mu^2\eta\frac{t}{R}[\frac{\xi_{11}^2}{8} + 4\xi_{20}\xi_{02}+2\xi_{11_o}(\frac{\xi_{11}}{8}+\frac{\xi_{02}}{2})]$$

$$F_{31} = \mu^2\eta\frac{t}{R}[\frac{2}{3}\xi_{11}\xi_{20}+2\xi_{11_o}(\frac{\xi_{20}}{3}+\frac{\xi_{11}}{12})]$$

$$F_{13} = \mu^2\eta\,\frac{t}{R}[\xi_{11}\xi_{02} + \xi_{11_o}\xi_{02}]$$

$$H_{20} = \mu^2\eta\,\frac{t}{R}[\frac{\xi_{11}^2}{8} + \xi_{11_o}\,\frac{\xi_{11}}{4}) - \mu^2\,\frac{t}{R}\,\xi_{20}$$

$$H_{11} = \mu^2\eta\,\frac{t}{R}[\xi_{11}\xi_{02} + \xi_{11_o}\xi_{02}] - \mu^2\,\frac{t}{R}\,\xi_{11}$$

$$H_{22} = \mu^2\eta\,\frac{t}{R}[-\frac{\xi_{11}^2}{8} - \xi_{11_o}\,\frac{\xi_{11}}{4}]$$

$$H_{31} = 0$$

$$H_{13} = \mu^2\eta\,\frac{t}{R}[-\xi_{11}\xi_{02} - \xi_{11_o}\xi_{02}]$$

In the above, the substitution $\xi_{20_o} = \xi_{11_o}/4$ has been made for convenience based on the postbuckling analysis results presented in reference 29. It is of interest to note that the same assumption has been utilized by Tennyson et al. in reference 21 in conjunction with an elastic analysis of the buckling process for compressed cylinders.

The equations found from the vanishing of the first variation can be reduced to four equations in the four unknowns ξ_{11}, ξ_{20}, ξ_{02}, and σ/E. This set of nonlinear algebraic equations can now be solved numerically for given values of the parameters Δ, μ, and η, and the relationship between $\sigma R/Et$ and eR/t can be obtained. Curves of $\sigma R/Et$ vs. eR/t are given in Figure 7.

UNCLASSIFIED

Security Classification

DOCUMENT CONTROL DATA - R & D

(Security classification of title, body of abstract and indexing annotation must be entered when the overall report is classified)

1. ORIGINATING ACTIVITY (Corporate author) Stanford University Department of Aeronautics and Astronautics Stanford, California	2a. REPORT SECURITY CLASSIFICATION UNCLASSIFIED 2b. GROUP N/A

3. REPORT TITLE

THE MAXIMUM STRENGTH OF INITIALLY IMPERFECT, AXIALLY COMPRESSED, CIRCULAR CYLINDRICAL SHELLS

4. DESCRIPTIVE NOTES (Type of report and inclusive dates)

Final Technical Report

5. AUTHOR(S) (First name, middle initial, last name)

Jean Mayers
Donald L. Wesenberg

6. REPORT DATE	7a. TOTAL NO. OF PAGES	7b. NO. OF REFS
August 1969	66	29

8a. CONTRACT OR GRANT NO.	9a. ORIGINATOR'S REPORT NUMBER(S)
DAAJ02-68-C-0035 b. PROJECT NO. Task 1F162204A17002 c. d.	USAAVLABS Technical Report 69-60 9b. OTHER REPORT NO(S) (Any other numbers that may be assigned this report)

10. DISTRIBUTION STATEMENT

This document is subject to special export controls, and each transmittal to foreign governments or foreign nationals may be made only with prior approval of US Army Aviation Materiel Laboratories, Fort Eustis, Virginia 23604.

11. SUPPLEMENTARY NOTES	12. SPONSORING MILITARY ACTIVITY
	U.S. Army Aviation Materiel Laboratories Fort Eustis, Virginia

13. ABSTRACT

The maximum strength of initially imperfect, axially compressed, circular cylindrical shells has been studied with the use of Reissner's variational principle, von Kármán-Donnell shell theory, and a deformation theory of plasticity. The results of the present analysis reflect families of load-end shortening curves for long circular cylinders. For a given material, each curve relates not only to an imperfection parameter which provides a loading path into the inelastic range but also to the radius-to-wall thickness ratio. Significant maximum strength reductions are obtained, relative to predictions based on linear-elastic theory, for specific materials in the range of radius-to-thickness ratios of practical interest.

DD FORM 1 NOV 68 1473 REPLACES DD FORM 1473, 1 JAN 64, WHICH IS OBSOLETE FOR ARMY USE.

UNCLASSIFIED

Security Classification

14. KEY WORDS	LINK A		LINK B		LINK C	
	ROLE	WT	ROLE	WT	ROLE	WT
Shell Structures Stability Maximum Strength Failure Analysis Plasticity Stiffened and Sandwich Construction						